**NTNU – Trondheim**
Norwegian University of
Science and Technology

# Simulation of Ultrafast Pump-Probe Measurements for Semiconductors

Johannes F Reinertsen

Nanotechnology
Submission date: June 2012
Supervisor: Ulf Lennart Østerberg, IET

Norwegian University of Science and Technology
Department of Electronics and Telecommunications

**Abstract**

Ultrafast pump-probe spectroscopy is a powerful technique for measuring decay times for an optically excited system, e.g. a semiconductor, on the pico- to femtosecond time scale. We present both a classical approach and a quantum mechanical density matrix approach to simulate the pump-probe signal and compare the two. The main features of a typical pump-probe experiment are explained and the "coherent artifact" is accounted for. With a three-level density matrix approach we explain some experimental features from pump-probe studies of gallium arsenide (GaAs). A simple model for simulating pump-probe of semiconductors is introduced, and the relation to the density matrix approach is derived. We also show how the semiconductor model reproduces the main features of experimental data from pump-probe studies of GaAs.

## Sammendrag

Ultrarask pump-probe-spektroskopi er en kraftfull teknikk for å måle relaksasjonstider for et optisk eksitert system, f.eks. en halvleder, på tidsskalaen pico- til femtosekunder. Vi presenterer både en klassisk tilnærming og en kvantemekanisk tetthetsmatrise-tilnærming for å simulere pump-probe-signalet, og sammenligner de to. Hovedtrekkene i et typisk pump-probe-eksperiment blir forklart, og "koherensartefakten" blir gjort rede for. Med en tre-nivå tetthetsmatrise-tilnærming forklarer vi noen eksperimentelle trekk fra pump-probe-studier av galliumarsenid (GaAs). En enkel modell for å simulere pump-probe av halvledere blir introdusert, og forbindelsen til tetthetsmatrise-tilnærmingen blir utledet. Vi viser også hvordan halvledermodellen gjenskaper hovedtrekkene i eksperimentelle data fra pump-probe-studier av GaAs.

# Preface

This report marks the end of five years as a student at NTNU. During my education towards a master in nanotechnology, I have encountered diverse subjects in a range of disciplines. I eventually developed an interest in electromagnetism and renewable energy, as well as a tiny bit of the "save the world"-syndrome. This led to a hope of one day to participate in the development of new solar cell technology.

After mixed experience with experimental lab work, I was determined to do a theoretical study for my master thesis. This led to a project on ultrafast pump-probe spectroscopy, which although not directly related to solar cell development, is a powerful technique than can be applied to semiconductor materials relevant in solar research.

The majority of this report is used to explain general features of pump-probe spectroscopy. Towards the end however, the focus is shifted to semiconductors specifically, and comparisons to experimental pump-probe results of gallium arsenide are made.

I would like to thank my supervisor, Prof. Ulf Österberg, for the guidance, advice and rewarding discussions provided during the work with this master thesis, as well as the project assignment last fall. Despite having much on his plate, he is always sincerely interested in his students' projects, and has a great insight in their current work.

*Trondheim,*
*June 2012*

*Johannes F. Reinertsen*

# Contents

# 1. Introduction

## 1.1. Semiconductors

Semiconductors are of great importance in modern electronics. A wide range of properties can be obtained by choosing the correct semiconductor and appropriately doping it with another material or designing microscopic geometries such as rods or multilayer stacks. These properties are used in e.g. computer components, lasers and solar cells.

In pushing the performance of computer technology, super fast current modulation is a key point, resulting in high demands on component design and properties. In today's gigahertz regime, operating speeds are approaching fundamental material limits. Investigating semiconductors' electronic responses on pico- and femtosecond time scales is therefore essential in meeting the requirements for new technology.

Material response is also important for semiconductors used in solar cells. Investigating the dynamics of electron energy transitions and scattering mechanisms in semiconductors can help optimizing solar cell design to increase their efficiency.

## 1.2. Ultrafast Pump-Probe Spectroscopy

Electromagnetic pulses are usually considered to be "ultrafast" when they are on the picosecond time scale or below. The needs for such short light pulses might not be obvious, but short bursts of light have been used to capture information on fast events since the 1850's [1]. It was realized that as long as the interaction between the light and the system investigated is sufficiently short, it does not matter how slow the detection systems are. In this way, high speed images can be produced without fast camera shutters, as long as a short enough flash is used (in an otherwise dark environment). A too long light pulse however, will tend to blur the image, as the event evolves considerably during the duration of the pulse. All these principles are transferable to the technique known as pump-probe spectroscopy, except the "image" is rather an intensity measurement or spectrum of the system investigated.

Ultrashort pulses are also used in a wide range of other applications such as optical communications, where the speed of data transfer is determined by the length of one light pulse, and materials processing, where short but intense pulses are favourable in cutting and drilling with a laser in heat sensitive materials [2].

Pump-probe spectroscopy is used to study dynamical processes in chemical, solid state and biological materials where light can induce a change in material properties. In semiconductors for example, charge carrier dynamics can be investigated by exciting the material with a laser [3]. With different configurations of the experimental set-up, differ-

ent material properties such as refractive index, birefringence or material structure can be measured [2].

The principle of pump-probe spectroscopy, as illustrated in figure 1.1, is fairly simple. An intense laser pulse termed pump arrives at the sample at a time $t_0$, and interacts with the sample in a way that changes some property of the sample. When the second pulse, termed probe or test, arrives at a later time $t_0 + \tau$, its interaction with the sample will reflect this property change. By varying the time delay $\tau$, the relaxation of the perturbation induced by the pump can be mapped out by detecting the outgoing probe signal. A key point here is that the pulses have to produce a short enough pulse/sample interaction, to not "blur" the result, so to speak. "Short enough" means that the pulse duration has to be in the same order of magnitude as the relaxation time of the sample (and preferably shorter), so that the system does not have time to evolve considerably during the interaction.

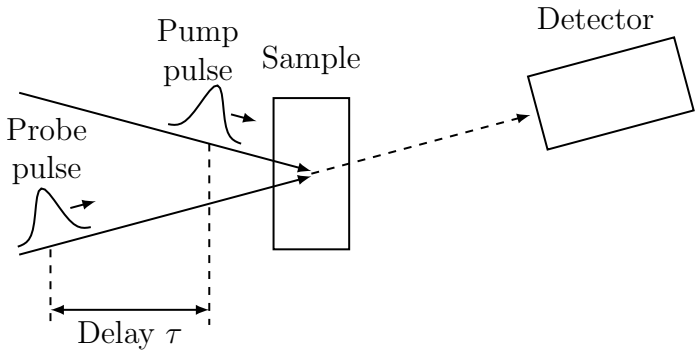


Figure 1.1.: Schematic overview of the pump-probe technique.

Figure 1.1 illustrates a simple pump-probe set-up, where transmission of the probe is measured to detect the absorption change of the sample induced by the pump pulse. In this set-up, the intense pump pulse excites the sample, suppressing the absorption of the probe pulse arriving shortly afterwards. This allows for probing of relaxation out of photoexited energy states. For long delay times $\tau$, the sample will eventually regain its equilibrium configuration before the probe arrives, and with a sufficient delay the transmitted probe signal will be as if no pump hit the sample. Most commonly, a slow detector measuring the time-integrated transmitted probe signal is used. The time resolution of the experiment is therefore determined by pulse durations.

In this study we will consider transmission mode pump-probe spectroscopy. This requires thin or diluted samples to prevent propagation effects which will give more complex signals, harder to interpret. Another option is to use a reflection set-up, where the reflected probe is measured rather than the transmitted. The principles of this set-up are mainly the same, bit without the demand for a thin sample. Additional surface effects may however come into play.

The simplest way to realize a pump-probe experiment is with a degenerate set-up, in which the beam from one laser is split into two. The probe is then led a longer distance than the pump before reaching the sample to get the desired delay $\tau$ between the two pulses. The probe is usually also attenuated so that it does not upset the current state

of the sample, but in fact only probes it.

An alternative to the degenerate case is to manipulate one of the pulses before it reaches the sample, to obtain a non-degenerate measurement. In certain experiments a spectrally broad pulse is desired, rather than the typical transform-limited ultrafast pulse with a narrow spectrum. The advantage of this continuum pulse is the ability to probe the sample with a whole spectrum of frequencies. The transmitted probe signal is then spectrally resolved by a monochromator, and the sample response is acquired for different frequencies without having to adjust the laser. The continuum generation can be done by passing the probe through e.g. a jet of ethylene glycol [4]. The non-degenerate experiment can also be realized with two different synchronized lasers.

In this study we will investigate different approaches to the theory of pump-probe spectroscopy. The aim is, by simple means, to simulate and reproduce some of the features in a typical pump-probe experiment. In the end, we will compare with experimental data from pump-probe of GaAs.

# 2. Theory

Pump-probe spectroscopy depends on the nonlinear absorption of the probe pulse. We will therefore first present the theory of nonlinear optics and nonlinear absorption before moving on to the different theoretical approaches to pump-probe spectroscopy.

## 2.1. Nonlinear Optics

All optical media were long thought to be linear [5, ch. 21], characterized by a linear relation between the polarization and the electric field

$$P = \epsilon_0 \chi E, \tag{2.1}$$

where $\epsilon_0$ is the permittivity of free space, and $\chi$ is the linear electric susceptibility of the medium. A nonlinear dielectric medium on the other hand, will have some other relation between $P$ and $E$. The error in treating a nonlinear medium as linear is however not very large, and for small intensities in the electric field, the behaviour is virtually linear. Large enough intensity will on the other hand produce nonlinear effects in any material. With small deviations from linear behaviour, it is common to expand the polarization in a Taylor series about $E$,

$$P = \epsilon_0 \chi^{(1)} E + \epsilon_0 \chi^{(2)} E^2 + \epsilon_0 \chi^{(3)} E^3 + \dots \tag{2.2}$$

For weak fields, the first term will dominate, regaining equation (2.1), while the effects of the following terms, denoted the second/third/etc. order nonlinearities, will become evident with strong field intensities.

In centrosymmetric media, the properties of the medium is not changed by the $\mathbf{r} \to -\mathbf{r}$ transformation. The reversal of $E$ should therefore result in the reversal of $P$. This is only true if every even order susceptibility is zero. We will thus neglect the second order nonlinearity $\epsilon_0 \chi^{(2)} E^2$ in the following. The first nonlinear term contributing to the polarization is then the third order polarization $\epsilon_0 \chi^{(3)} E^3$, which will be dominating the nonlinear behaviour of the medium.

With a monochromatic wave,

$$E(t) = \frac{1}{2} E_0 \left( e^{i(\mathbf{k}\cdot\mathbf{r} - \omega t)} + e^{-i(\mathbf{k}\cdot\mathbf{r} - \omega t)} \right), \tag{2.3}$$

incident on the nonlinear medium, the nonlinear polarization will be given as

$$\begin{aligned} P^{(3)}(t) = \epsilon_0 \chi^{(3)} E(t)^3 = {} & \frac{3}{4} \epsilon_0 \chi^{(3)} E_0^3 \left( e^{i(\mathbf{k}\cdot\mathbf{r} - \omega t)} + e^{-i(\mathbf{k}\cdot\mathbf{r} - \omega t)} \right) \\ & + \frac{1}{4} \epsilon_0 \chi^{(3)} E_0^3 \left( e^{3i(\mathbf{k}\cdot\mathbf{r} - \omega t)} + e^{-3i(\mathbf{k}\cdot\mathbf{r} - \omega t)} \right), \end{aligned} \tag{2.4}$$

which shows that light with three times the frequency $\omega$ of the incident light is generated. The yield of the third-harmonic light when considering propagation through the medium is however low. In addition, the third-harmonic light will propagate in the direction $3\mathbf{k}$ while the geometry of the pump-probe experiment as shown in figure 1.1 only detects the light propagating in the direction of the probe, $\mathbf{k}$. With these assumptions, the third order polarization of interest to us simplifies to

$$P^{(3)}(t) = \epsilon_0 \chi^{(3)} |\mathcal{E}(t)|^2 E(t), \tag{2.5}$$

where $\mathcal{E}(t)$ is the complex electric field with the property $|\mathcal{E}(t)|^2 = E_0^2$.

### 2.1.1. Time-Varying Fields

The result in equation (2.5) is valid for a constant, monochromatic electric field $E(t)$. In this case, the field has only one frequency $\omega$, and the susceptibility $\chi^{(3)}$, which in general is frequency dependent can be treated as a constant. When treating a time-varying field, especially an ultrafast pulse, the field will inherently consist of different frequencies. In the frequency domain, the linear polarization is simply given as the product of the electric field and the frequency dependent susceptibility

$$P(\omega) = \epsilon_0 \chi(\omega) E(\omega), \tag{2.6}$$

or written in a complex notation,

$$\mathcal{P}(\omega) = \epsilon_0 \chi(\omega) \mathcal{E}(\omega). \tag{2.7}$$

In this case, $\chi(\omega)$ can be complex, with the real part corresponding to refraction of the electric field, and the imaginary part corresponding to absorption of the field.

With an inverse Fourier transform, the linear polarization in the time domain becomes

$$\mathcal{P}(t) = \epsilon_0 \int R(t - t') \mathcal{E}(t') dt', \tag{2.8}$$

the convolution of the electric field and the response function of the medium $R(t)$, where $R(t)$ is the inverse Fourier transform of $\chi(\omega)$. The third order polarization is similarly given, in the time domain, as

$$\mathcal{P}^{(3)}(t) = \epsilon_0 \int R^{(3)}(t - t') |\mathcal{E}(t')|^2 \mathcal{E}(t') dt', \tag{2.9}$$

where higher frequency terms are still neglected.

For the system to be causal, the response function $R(t)$ has to be zero for all times $t < 0$. $R(t)$ is therefore often represented as the Heaviside unit step function $\Theta(t)$ multiplied with a function governing the response for $t > 0$. The step function is defined as

$$\Theta(t) = \begin{cases} 0, & t < 0, \\ 1, & t > 0. \end{cases} \tag{2.10}$$

### 2.1.2. Nonlinear Absorption

We will next show how the intensity of the field emerging from the medium depends on the induced nonlinear polarization. This nonlinear intensity change or absorption is what is measured in the pump-probe experiment. The approach is similar to that of Shen [6, ch. 3] and Mukamel [7, ch. 4].

We begin with two of Maxwell's equations in a homogeneous, non-magnetic medium:

$$\nabla \times H = \epsilon_0 \frac{dE}{dt} + \frac{dP}{dt}, \tag{2.11}$$

$$\nabla \times E = -\mu_0 \frac{dH}{dt}. \tag{2.12}$$

By applying the curl operator to equation (2.12) we get

$$\nabla \times (\nabla \times E) = -\nabla \times \mu_0 \frac{dH}{dt}, \tag{2.13}$$

$$-\nabla^2 E = -\mu_0 \frac{d}{dt}(\nabla \times H). \tag{2.14}$$

Inserting equation (2.11) gives

$$-\nabla^2 E = -\mu_0 \epsilon_0 \frac{d^2 E}{dt^2} - \mu_0 \frac{d^2 P}{dt^2}, \tag{2.15}$$

or

$$\boxed{\nabla^2 E - \frac{1}{c^2}\frac{d^2 E}{dt^2} = \mu_0 \frac{d^2 P}{dt^2},} \tag{2.16}$$

which is the wave equation for an electric field in a polarizable medium. We divide the polarization into a linear part $P_{\mathrm{L}}$ and a non-linear part $P_{\mathrm{NL}}$, where $P_{\mathrm{L}} = \epsilon_0(\epsilon_r - 1)E$ to get

$$\nabla^2 E - \frac{1}{c^2}\frac{d^2 E}{dt^2} = \frac{\epsilon_r - 1}{c^2}\frac{d^2 E}{dt^2} + \mu_0 \frac{d^2 P_{\mathrm{NL}}}{dt^2}. \tag{2.17}$$

In a non-magnetic material, $n \approx \sqrt{\epsilon_r}$, and

$$\nabla^2 E - \frac{n^2}{c^2}\frac{d^2 E}{dt^2} = \mu_0 \frac{d^2 P_{\mathrm{NL}}}{dt^2}. \tag{2.18}$$

We next evaluate the complex electric field and polarization, writing both as harmonic waves propagating in the $z$-direction, modulated by a slowly varying envelope:

$$\mathcal{E}(z,t) = a_E(z,t)e^{i(kz-\omega_c t)}, \tag{2.19}$$

$$\mathcal{P}_{\mathrm{NL}}(z,t) = a_P(z,t)e^{i(kz-\omega_c t)}, \tag{2.20}$$

where $a_{E/P}$ is a slowly varying envelope function. Treating $a_{E/P}$ as constant in time, also known as the slowly varying envelope approximation (SVEA), equation (2.18) becomes

$$\nabla^2 \mathcal{E} + \omega_c^2 \frac{n^2}{c^2}\mathcal{E} = -\omega_c^2 \mu_0 \mathcal{P}_{\mathrm{NL}}. \tag{2.21}$$

Expanding the Laplacian gives

$$e^{i(kz-\omega_c t)}\left(\frac{\partial^2}{\partial z^2}+2ik\frac{\partial}{\partial z}-k^2+\omega_c^2\frac{n^2}{c^2}\right)a_E(z,t)=-\omega_c^2\mu_0 a_P(z,t)e^{i(kz-\omega_c t)}. \tag{2.22}$$

With $k=\omega_c n/c$ and assuming

$$\left|\frac{\partial^2 a_E(z,t)}{\partial z^2}\right| \ll \left|k\frac{\partial a_E(z,t)}{\partial z}\right|, \tag{2.23}$$

we get

$$2ik\frac{\partial a_E(z,t)}{\partial z}=-\omega_c^2\mu_0 a_P(z,t), \tag{2.24}$$

or

$$\frac{\partial a_E(z,t)}{\partial z}=\frac{i\omega_c}{2cn\epsilon_0}a_P(z,t). \tag{2.25}$$

With a thin sample, we assume the envelope of the polarization to be constant through the sample. We can then easily evaluate the integral

$$\int_0^l \partial a_E(z,t)=\frac{i\omega_c}{2cn\epsilon_0}\int_0^l a_P(t)\partial z, \tag{2.26}$$

governing the fields in a thin sample placed between $z=0$ and $z=l$, to get

$$a_E(l,t)=a_E(0,t)+\frac{i\omega_c l}{2cn\epsilon_0}a_P(t). \tag{2.27}$$

The electric field emerging from the sample (at $z=l$) is similarly

$$\mathcal{E}_{\text{out}}(t;\tau)=\mathcal{E}_{\text{in}}(t)+\frac{i\omega_c l}{2cn\epsilon_0}\mathcal{P}_{\text{NL}}(t;\tau), \tag{2.28}$$

where we have added $\tau$-dependency in the polarization and output field, $\tau$ being the delay between pump and probe pulse in the pump-probe experiment.

When measuring the pump-probe signal, the intensity is as usual proportional to the absolute square of the complex electric field $\mathcal{E}_{\text{out}}(t)$:

$$\begin{aligned} I(t;\tau) &\propto \left|\mathcal{E}_{\text{in}}(t)+\frac{i\omega_c l}{2cn\epsilon_0}\mathcal{P}_{\text{NL}}(t;\tau)\right|^2 \\ &\propto \left|\mathcal{E}_{\text{in}}(t)\right|^2+\frac{\omega_c l}{cn\epsilon_0}\text{Im}\left\{\mathcal{E}_{\text{in}}(t)\mathcal{P}^*_{\text{NL}}(t;\tau)\right\}+\left(\frac{\omega_c l}{2cn\epsilon_0}\right)^2\left|\mathcal{P}_{\text{NL}}(t;\tau)\right|^2. \end{aligned} \tag{2.29}$$

$|\mathcal{P}_{\text{NL}}(t;\tau)|^2$ will be small compared to the other terms, so by neglecting this term, and subtracting the constant signal from the incident field $|\mathcal{E}_{\text{in}}(t)|^2$, we get the differential intensity

$$\Delta I(t;\tau)\propto \text{Im}\left\{\mathcal{E}_{\text{in}}(t)\mathcal{P}^{(3)*}(t;\tau)\right\}. \tag{2.30}$$

We have inserted $P^{(3)}$ for $P_{\mathrm{NL}}$ as this is the dominating nonlinear term as explained above. With a slow integrating detector, the signal detected is the differential energy

$$\boxed{\Delta U(\tau) \propto \int dt \, \mathrm{Im}\left\{\mathcal{E}_{\mathrm{in}}(t)\mathcal{P}^{(3)*}(t;\tau)\right\}.} \tag{2.31}$$

We can also choose to evaluate the Fourier transform of equation (2.28):

$$\mathcal{E}_{\mathrm{out}}(\omega;\tau) = \mathcal{E}_{\mathrm{in}}(\omega) + \frac{i\omega_c l}{2cn\epsilon_0}\mathcal{P}_{\mathrm{NL}}(\omega;\tau), \tag{2.32}$$

to get the spectrally resolved differential intensity

$$\boxed{\Delta I(\omega;\tau) \propto \mathrm{Im}\left\{\mathcal{E}_{\mathrm{in}}(\omega)\mathcal{P}^{(3)*}(\omega;\tau)\right\}.} \tag{2.33}$$

Integrating this expression over all frequencies will give the same result for the differential detected energy $\Delta U(\tau)$ as equation the above according to Parseval's theorem: If $F(\omega)$ and $G(\omega)$ are the respective Fourier transforms of $f(t)$ and $g(t)$ then

$$\int_{-\infty}^{\infty} d\omega \, F(\omega)G^*(\omega) = \int_{-\infty}^{\infty} dt \, f(t)g^*(t). \tag{2.34}$$

## 2.2. Classical Approach to Pump-Probe Spectroscopy

We first treat the pump-probe experiment classically, with an approach close to that of Weiner [2]. In finding the third order polarization necessary to find the pump-probe signal, we begin with the expression from section 2.1.1:

$$\mathcal{P}^{(3)}(t) = \epsilon_0 \int R^{(3)}(t-t')|\mathcal{E}(t')|^2\mathcal{E}(t')dt'. \tag{2.35}$$

This can be rewritten to simplify the derivation to follow by assuming a broad-band on-resonance absorption process.

In a resonant dielectric medium, the susceptibility close to resonance is typically given as [5, ch. 5]

$$\chi^{(3)}(\omega) \propto \frac{\omega - \omega_{\mathrm{r}} - i\Delta\omega/2}{(\omega-\omega_{\mathrm{r}})^2 + (\Delta\omega/2)^2}, \tag{2.36}$$

where the imaginary part, responsible for absorption is a Lorentzian centered at the resonance of the system, $\omega_{\mathrm{r}}$. An inverse Fourier transform gives the response function

$$R^{(3)}(t) = iA^{(3)}(t)e^{-i\omega_{\mathrm{r}}t}, \tag{2.37}$$

where

$$A^{(3)}(t) = \Theta(t)e^{-\Delta\omega/2\cdot t} = \Theta(t)e^{-t/\tau_{\mathrm{R}}}, \tag{2.38}$$

governs the on-resonance decay of the system. $A^{(3)}(t)$ is the unit step function times an exponentially decaying function with a characteristic time $\tau_{\mathrm{R}}$ determining the decay

time of the system. In the case of broad-band absorption, $\Delta\omega$ is large, giving a short characteristic decay time $\tau_{\mathrm{R}}$. $A^{(3)}(t)$ is thus a narrow function in time.

We write the field as

$$\mathcal{E}(t) = a(t)e^{-i\omega_E t}, \tag{2.39}$$

where $a(t)$ is a slowly varying envelope function modulating the harmonic field. In the on-resonance case, we have $\omega_E = \omega_{\mathrm{r}}$ and equation (2.35) becomes

$$\mathcal{P}^{(3)}(t) = \epsilon_0 \int iA^{(3)}(t-t')e^{-i\omega_E(t-t')}|\mathcal{E}(t')|^2 a(t')e^{-i\omega_E t'}dt'. \tag{2.40}$$

When $A^{(3)}(t)$ is a narrow function in time, only small values of $t - t'$ will contribute to the integral. Thus $a(t') \approx a(t)$ in the integrand, giving

$$\begin{aligned}\mathcal{P}^{(3)}(t) &= \epsilon_0 \int iA^{(3)}(t-t')e^{-i\omega_E(t-t')}|\mathcal{E}(t')|^2 a(t)e^{-i\omega_E t'}dt' \\ &= \epsilon_0 a(t)e^{-i\omega_E t}\int iA^{(3)}(t-t')|\mathcal{E}(t')|^2 dt' \\ &= \epsilon_0 \mathcal{E}(t)\int iA^{(3)}(t-t')|\mathcal{E}(t')|^2 dt'.\end{aligned} \tag{2.41}$$

### 2.2.1. Pump-Probe Signal

The pump (P) and probe (test, T) fields are, as in the experimental set-up, propagating along different vectors $\mathbf{k}_{\mathrm{P}}$ and $\mathbf{k}_{\mathrm{T}}$. We write the complex pump and probe fields as

$$\mathcal{E}_{\mathrm{P}}(r,t) = a_{\mathrm{P}}(t)e^{i(\mathbf{k}_{\mathrm{P}}\cdot\mathbf{r}-\omega_{\mathrm{P}}t)}, \tag{2.42}$$

$$\mathcal{E}_{\mathrm{T}}(r,t) = a_{\mathrm{T}}(t)e^{i(\mathbf{k}_{\mathrm{T}}\cdot\mathbf{r}-\omega_{\mathrm{T}}(t-\tau))}, \tag{2.43}$$

where $a_{\mathrm{P/T}}(t)$ are slowly varying envelope functions. In the degenerate case, we have $\omega_{\mathrm{T}} = \omega_{\mathrm{P}}$ and $a_{\mathrm{T}}(t) = a_{\mathrm{P}}(t-\tau)$, where $\tau$ is the delay between pump and probe pulse.

In the pump-probe experiment, the detector only measures fields propagating in the same direction as the probe pulse, i.e. $\mathbf{k}_{\mathrm{T}}$. For the induced polarization to be measured, it therefore has to radiate a field in this direction. When inserting the total field, which is the sum of equations (2.42) and (2.43) into equation (2.41), the only terms propagating in the $\mathbf{k}_{\mathrm{T}}$ direction are

$$\begin{aligned}\mathcal{P}^{(3)}(t) = \epsilon_0\mathcal{E}_{\mathrm{T}}(t)\int iA^{(3)}(t-t')\mathcal{E}_{\mathrm{P}}(t')^*\mathcal{E}_{\mathrm{P}}(t')dt' \\ + \epsilon_0\mathcal{E}_{\mathrm{P}}(t)\int iA^{(3)}(t-t')\mathcal{E}_{\mathrm{P}}(t')^*\mathcal{E}_{\mathrm{T}}(t')dt',\end{aligned} \tag{2.44}$$

when terms of higher order in the weak probe field are ignored. Inserting this in equation (2.31), gives the energy readout of the detector

$$\begin{aligned}\Delta U(\tau) \propto \int dt \mathrm{Im}\left\{|\mathcal{E}_{\mathrm{T}}(t)|^2\int dt' iA^{(3)}(t-t')|\mathcal{E}_{\mathrm{P}}(t')|^2\right\} \\ + \int dt \mathrm{Im}\left\{\mathcal{E}_{\mathrm{T}}(t)\mathcal{E}_{\mathrm{P}}^*(t)\int dt' iA^{(3)}(t-t')\mathcal{E}_{\mathrm{P}}(t')\mathcal{E}_{\mathrm{T}}(t')^*\right\}.\end{aligned} \tag{2.45}$$

As $A^{(3)}(t)$ is a real function, we get

$$\Delta U(\tau) \propto \int dt |\mathcal{E}_{\mathrm{T}}(t)|^2 \int dt' A^{(3)}(t-t') |\mathcal{E}_{\mathrm{P}}(t')|^2 + \frac{1}{2} \int dt \mathcal{E}_{\mathrm{T}}(t) \mathcal{E}_{\mathrm{P}}^*(t) \int dt' A^{(3)}(t-t') \mathcal{E}_{\mathrm{P}}(t') \mathcal{E}_{\mathrm{T}}(t')^* + \text{c.c.} \tag{2.46}$$

The two terms are commonly denoted $\gamma(\tau)$ and $\beta(\tau)$, first introduced by Ippen and Shank [8]. We thus write $\Delta U(\tau) \propto \gamma(\tau) + \beta(\tau)$, with

$$\gamma(\tau) = \int dt |\mathcal{E}_{\mathrm{T}}(t)|^2 \int dt' A^{(3)}(t-t') |\mathcal{E}_{\mathrm{P}}(t')|^2. \tag{2.47}$$

In the degenerate case, we can rewrite this as

$$\begin{aligned} \gamma(\tau) &= \int dt |\mathcal{E}_{\mathrm{P}}(t-\tau)|^2 \int dt' A^{(3)}(t') |\mathcal{E}_{\mathrm{P}}(t-t')|^2 \\ &= \int dt' A^{(3)}(t') \int dt |\mathcal{E}_{\mathrm{P}}(t-\tau)|^2 |\mathcal{E}_{\mathrm{P}}(t-t')|^2, \end{aligned} \tag{2.48}$$

and with the change of variables $t \to t + \tau$ and $t' \to -t' + \tau$, we get

$$\boxed{\gamma(\tau) = \int dt' A^{(3)}(\tau - t') \int dt |\mathcal{E}_{\mathrm{P}}(t)|^2 |\mathcal{E}_{\mathrm{P}}(t'+t)|^2,} \tag{2.49}$$

which is the third order response function convolved with the intensity autocorrelation function of the electric field.

$\beta(\tau)$ is given as

$$\boxed{\beta(\tau) = \frac{1}{2} \int dt \left\{ \mathcal{E}_{\mathrm{T}}(t) \mathcal{E}_{\mathrm{P}}^*(t) \int dt' A^{(3)}(t-t') \mathcal{E}_{\mathrm{P}}(t') \mathcal{E}_{\mathrm{T}}^*(t') + \text{c.c.} \right\}.} \tag{2.50}$$

This contribution is known as the "coherent coupling term". It results from the two pulses, when temporally overlapping, creating an induced absorption grating which scatters some of the pump intensity in the direction of the probe. The $\beta(\tau)$ contribution will give a coherent coupling artifact in the measured pump-probe signal for short time delays $\tau$, when there is large temporal overlap of the two pulses. At zero delay time, the pump and probe pulses are indistinguishable in a degenerate experiment, and the contributions from the $\gamma(t)$ and $\beta(t)$ terms are equal as evident from the expressions given.

The coherent contribution to the pump-probe signal can be reduced by reducing the coherence of the pulses as we will show in section 2.2.1. The amplitude of the coherent artifact is also depending on the polarization orientation of the two pulses, which has not been treated here. It has been shown that polarizing the probe pulse perpendicular to the pump pulse greatly reduces the coherent artifact in some cases [9, 3]. In other materials however, the ratio between the coherent term and the saturation term remains constant when comparing perpendicular to parallel polarization [9].

We next evaluate the pump-probe signal through the expressions for $\gamma(\tau)$ and $\beta(\tau)$ for two limiting cases of the third order response function: The delta function and the unit step function.

### $\mathbf{A^{(3)}(t)}$ as a Delta-Function

When absorption dynamics in the system occur very fast compared to pulse durations, the response function can be modelled by a delta-function. The expressions for $\gamma(\tau)$ and $\beta(\tau)$ then turns into

$$\begin{aligned}\gamma(\tau) &= \int dt' \delta(\tau - t') \int dt |\mathcal{E}_{\mathrm{P}}(t)|^2 |\mathcal{E}_{\mathrm{P}}(t'+t)|^2 \\ &= \int dt |\mathcal{E}_{\mathrm{P}}(t)|^2 |\mathcal{E}_{\mathrm{P}}(\tau+t)|^2, \end{aligned} \tag{2.51}$$

and

$$\begin{aligned}\beta(\tau) &= \frac{1}{2} \int dt \left\{ \mathcal{E}_{\mathrm{T}}(t) \mathcal{E}_{\mathrm{P}}^*(t) \int dt' \delta(t-t') \mathcal{E}_{\mathrm{P}}(t') \mathcal{E}_{\mathrm{T}}^*(t') + \mathrm{c.c.} \right\} \\ &= \frac{1}{2} \int dt \left\{ \mathcal{E}_{\mathrm{T}}(t) \mathcal{E}_{\mathrm{P}}^*(t) \mathcal{E}_{\mathrm{P}}(t) \mathcal{E}_{\mathrm{T}}^*(t) + \mathrm{c.c.} \right\} \\ &= \int dt |\mathcal{E}_{\mathrm{P}}(t)|^2 |\mathcal{E}_{\mathrm{T}}(t)|^2, \end{aligned} \tag{2.52}$$

which in the degenerate case becomes

$$\begin{aligned}\beta(\tau) &= \int dt |\mathcal{E}_{\mathrm{P}}(t)|^2 |\mathcal{E}_{\mathrm{P}}(t-\tau)|^2 \\ &= \int dt |\mathcal{E}_{\mathrm{P}}(t+\tau)|^2 |\mathcal{E}_{\mathrm{P}}(t)|^2, \end{aligned} \tag{2.53}$$

so that both contributions to the pump-probe signal are proportional to the intensity autocorrelation function, which means the only thing measured is pulse characteristics. The signals from the two contributions together with the total pump-probe signal are given in figure 2.1.

### $\mathbf{A^{(3)}(t)}$ as a Unit Step Function

If we assume the absorption response to have a very fast rise time, but a slow recovery, the response function can be approximated by a unit step function $\Theta(t)$. The contribution $\gamma(\tau)$ to the pump-probe signal is then

$$\begin{aligned}\gamma(\tau) &= \int dt' \Theta(\tau - t') \int dt |\mathcal{E}_{\mathrm{P}}(t)|^2 |\mathcal{E}_{\mathrm{P}}(t'+t)|^2 \\ &= \int_{-\infty}^{\tau} dt' \int dt |\mathcal{E}_{\mathrm{P}}(t)|^2 |\mathcal{E}_{\mathrm{P}}(t'+t)|^2, \end{aligned} \tag{2.54}$$

which is proportional to the cumulative intensity autocorrelation. $\beta(\tau)$, on the other hand, becomes

$$\begin{aligned}\beta(\tau) =& \frac{1}{2} \int dt\, \mathcal{E}_{\mathrm{T}}(t) \mathcal{E}_{\mathrm{P}}^*(t) \int dt' \Theta(t-t') \mathcal{E}_{\mathrm{P}}(t') \mathcal{E}_{\mathrm{T}}^*(t') \\ &+ \frac{1}{2} \int dt\, \mathcal{E}_{\mathrm{P}}(t) \mathcal{E}_{\mathrm{T}}^*(t) \int dt' \Theta(t-t') \mathcal{E}_{\mathrm{T}}(t') \mathcal{E}_{\mathrm{P}}^*(t'). \end{aligned} \tag{2.55}$$

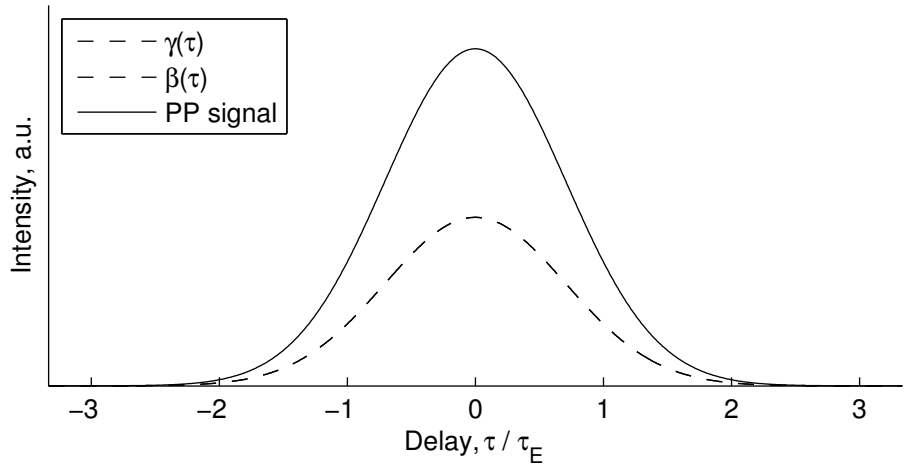


Figure 2.1.: The analytically evaluated pump-probe signal for a delta function response function. The two contributions are equal for all delay times $\tau$. Pulses are modelled as degenerate Gaussian pulses with constant frequency (no chirp).

We change the integration order in the last integral to obtain

$$\begin{aligned}\beta(\tau) =&\frac{1}{2}\int dt\, \mathcal{E}_{\mathrm{T}}(t)\mathcal{E}_{\mathrm{P}}^*(t)\int dt'\Theta(t-t')\mathcal{E}_{\mathrm{P}}(t')\mathcal{E}_{\mathrm{T}}^*(t')\\ &+\frac{1}{2}\int dt'\, \mathcal{E}_{\mathrm{T}}(t')\mathcal{E}_{\mathrm{P}}^*(t')\int dt\Theta(t-t')\mathcal{E}_{\mathrm{P}}(t)\mathcal{E}_{\mathrm{T}}^*(t).\end{aligned} \tag{2.56}$$

By exchanging the dummy variables $t$ and $t'$ in the last integral we get

$$\begin{aligned}\beta(\tau) =&\frac{1}{2}\int dt\, \mathcal{E}_{\mathrm{T}}(t)\mathcal{E}_{\mathrm{P}}^*(t)\int dt'\Theta(t-t')\mathcal{E}_{\mathrm{P}}(t')\mathcal{E}_{\mathrm{T}}^*(t')\\ &+\frac{1}{2}\int dt\, \mathcal{E}_{\mathrm{T}}(t)\mathcal{E}_{\mathrm{P}}^*(t)\int dt'\Theta(t'-t)\mathcal{E}_{\mathrm{P}}(t')\mathcal{E}_{\mathrm{T}}^*(t'),\end{aligned} \tag{2.57}$$

and when $\Theta(t)$ is the unit step function, the two terms add up to

$$\begin{aligned}\beta(\tau) =&\frac{1}{2}\int dt\, \mathcal{E}_{\mathrm{T}}(t)\mathcal{E}_{\mathrm{P}}^*(t)\int dt'\, \mathcal{E}_{\mathrm{P}}(t')\mathcal{E}_{\mathrm{T}}^*(t')\\ =&\frac{1}{2}\left|\int dt\, \mathcal{E}_{\mathrm{P}}(t)\mathcal{E}_{\mathrm{P}}^*(t-\tau)\right|^2,\end{aligned} \tag{2.58}$$

which is the electric field autocorrelation squared.

While $\beta(\tau)$ gives a transient signal, $\gamma(\tau)$ will contribute for all positive delay times. The two contributions together with the total pump-probe signal are shown in figure 2.2. As always, the contributions are equal at zero delay.

### Analytical Example: The Chirped Gaussian Pulse

We now evaluate the pump-probe signal for a specific pulse shape: The linearly chirped Gaussian pulse, given as

$$\mathcal{E}(t) = e^{-t^2/\tau_E^2}e^{i(\omega_E t+\beta t^2)}, \tag{2.59}$$

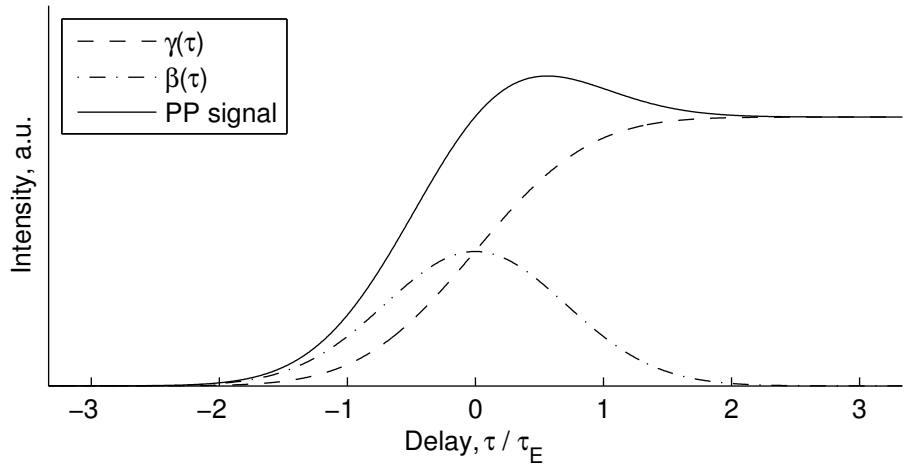


Figure 2.2.: The analytically evaluated pump-probe signal for a unit step function response function. Pulses are modelled as degenerate Gaussian pulses with constant frequency (no chirp).

and shown in figure 2.3. This simple mathematical representation is an easy way to simulate the properties of a short, spectrally broadened pulse, resembling the continuum pulse described in section 1.2. The pulse consists of a rapid oscillation with carrier frequency $\omega_E$ modulated by a Gaussian envelope with the characteristic time constant $\tau_E$. In addition, the chirp constant $\beta$ governs the instantaneous frequency of the field, increasing/decreasing the frequency along the pulse.

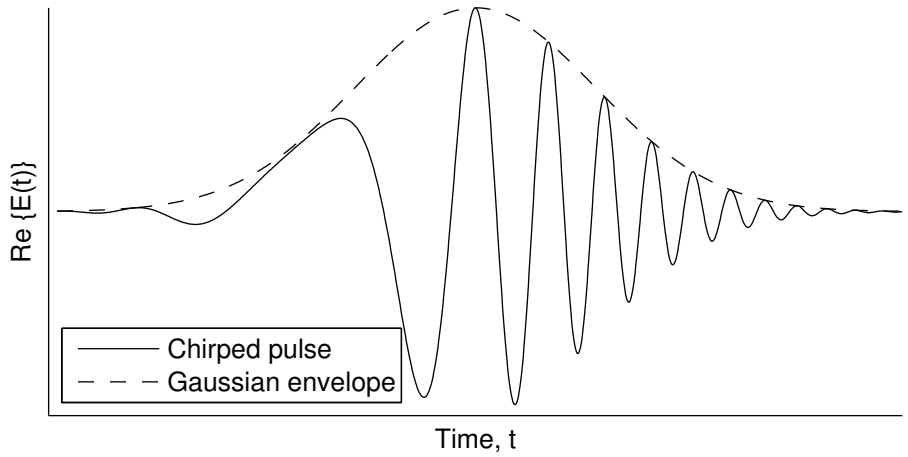


Figure 2.3.: Linearly chirped pulse and its Gaussian envelope.

As the general expression for $\gamma(\tau)$ only depends on $|E_{\mathrm{P/T}}(t)|^2$, which in turn only depends on $\tau_E$, neither carrier frequency nor chirp will affect the signal contribution from $\gamma(\tau)$ in the formalism developed earlier. Only the envelope of the pulse matters.

$\beta(\tau)$ on the other hand, depends on the coherence of the pulses, and will thus be

affected by the instantaneous frequency of the pulse. Considering the case of a unit step response function, we get the contribution from $\beta(\tau)$ to the pump-probe signal for a chirped pulse by combining equations (2.59) and (2.58) to give

$$\begin{aligned}\beta(\tau) &= \frac{1}{2}\left|\int dt\, e^{-t^2/\tau_E^2} e^{i(\omega_E t+\beta t^2)} e^{-(t-\tau)^2/\tau_E^2} e^{-i(\omega_E(t-\tau)+\beta(t-\tau)^2)}\right|^2 \\ &= \frac{1}{2}\left|e^{-\tau^2/4\tau_E^2} e^{i\omega_E\tau}\int dt\, e^{-(t-\tau/2)^2/\tau_E^2} e^{2i\beta\tau(t-\tau/2)}\right|^2 . \end{aligned} \tag{2.60}$$

Setting $t' = t - \tau/2$, we get

$$\begin{aligned}\beta(\tau) &= \frac{1}{2}\left|e^{-\tau^2/4\tau_E^2}\int dt'\, e^{-t'^2/\tau_E^2} e^{2i\beta\tau t'}\right|^2 \\ &= \frac{1}{2}\left|e^{-\tau^2/4\tau_E^2}\sqrt{\pi\tau_E^2}\, e^{-\tau_E^2\beta^2\tau^2}\right|^2 \\ &= \frac{\sqrt{\pi\tau_E^2}}{2} e^{-\tau^2(1/2\tau_E^2+2\tau_E^2\beta^2)}. \end{aligned} \tag{2.61}$$

We see that $\beta(\tau)$ is still a Gaussian function centered at $\tau = 0$, and that $\beta(0)$ is independent of the chirp, but by increasing the chirp coefficient $\beta$, we get a much faster decay in $\beta(\tau)$, making its contribution to the total pump-probe signal less dominant. This is illustrated in figure 2.4, which displays the total pump-probe signal for different chirp coefficients $\beta$. The result is not surprising, as the coherent signal relies on coherence between pump and probe pulse. When introducing chirp to the pulses, the coherence is reduced, resulting in a reduced coherent contribution to the total pump-probe signal.

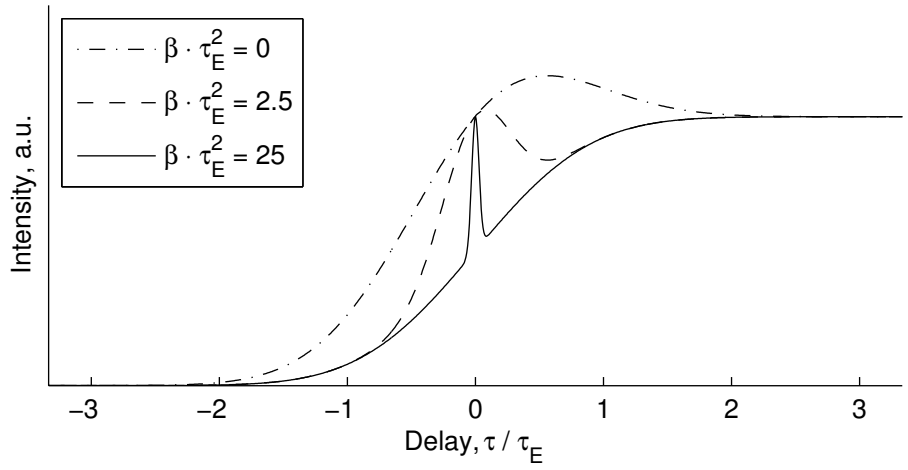


Figure 2.4.: The analytically evaluated pump-probe signal for a unit step function response function. Pulses are modelled as degenerate Gaussian pulses with different chirp coefficients $\beta$.

## 2.3. Density Matrix Approach to Pump-Probe Spectroscopy

We now look to a quantum mechanical evaluation of the pump-probe experiment. The approach is similar to that of Joffre [10], using a density matrix representation to describe the system investigated. We have thus assumed that only certain energy levels are allowed for the system. We assume the density operator $\rho$ to obey the Liouville equation [11, p. 655], written as

$$i\hbar\frac{\mathrm{d}\rho}{\mathrm{d}t} = [H_0, \rho] + [W(t), \rho] + i\hbar\left.\frac{\partial\rho}{\partial t}\right|_{\text{relax}}, \tag{2.62}$$

where $H_0$ is the unperturbed Hamiltonian, and $W(t) = -\mu E(t)$ is the dipolar interaction with the electric field. $\mu$ is the electric dipole operator. The eigenstates of $H_0$ are

$$H_0 \left|n\right\rangle = \hbar\omega_n \left|n\right\rangle . \tag{2.63}$$

The last term in (2.62) represents the relaxation of the system back to equilibrium, assumed to follow

$$\left.\frac{\partial\rho}{\partial t}\right|_{\text{relax}} = -\Gamma_{nm}\left(\rho_{nm} - \rho_{nm}^{\text{eq}}\right), \tag{2.64}$$

which leads to an exponential relaxation at a rate $\Gamma_{nm}$. In the following, we assume that the thermal energy of the system is much smaller than the transition energies, so that only the ground state is populated in equilibrium. (2.64) then turns into

$$\left.\frac{\partial\rho}{\partial t}\right|_{\text{relax}} = -\Gamma_{nm}\rho_{nm}, \tag{2.65}$$

where $\Gamma_{nm}$ is a population relaxation rate when $n = m$ and a dephasing rate when $n \neq m$. The inverses $(1/\Gamma_{nm})$ are known as characteristic decay times and dephasing times, often denoted $T_1$ and $T_2$ respectively.

We next evaluate the matrix elements of the first commutator in (2.62):

$$\begin{aligned}
\left\langle n\right| [H_0, \rho] \left|m\right\rangle &= \left\langle n\right| H_0\rho - \rho H_0 \left|m\right\rangle \\
&= \left\langle n\right| \hbar\omega_n\rho - \rho\hbar\omega_m \left|m\right\rangle \\
&= \hbar\omega_{nm} \left\langle n\right| \rho \left|m\right\rangle \\
&= \hbar\omega_{nm}\rho_{nm},
\end{aligned} \tag{2.66}$$

where $\omega_{nm}$ is the transition frequency $\omega_n - \omega_m$. The matrix elements of the second commutator are

$$\begin{aligned}
\left\langle n\right| [W, \rho] \left|m\right\rangle &= \left\langle n\right| W\rho - \rho W \left|m\right\rangle \\
&= -E(t)\left[\left\langle n\right| \mu\rho \left|m\right\rangle - \left\langle n\right| \rho\mu \left|m\right\rangle\right] \\
&= -E(t)\sum_l \left[\mu_{nl}\rho_{lm} - \rho_{nl}\mu_{lm}\right].
\end{aligned} \tag{2.67}$$

The evolution equation of the density matrix elements can therefore be written as

$$-\left(\frac{\mathrm{d}}{\mathrm{d}t}+i\omega_{nm}+\Gamma_{nm}\right)i\hbar\rho_{nm}(t)=E(t)\sum_l\left[\mu_{nl}\rho_{lm}(t)-\rho_{nl}(t)\mu_{lm}\right]. \tag{2.68}$$

We solve this by defining the Green's function $G_{nm}(t)$ such that it fulfills

$$-\left(\frac{\mathrm{d}}{\mathrm{d}t}+i\omega_{nm}+\Gamma_{nm}\right)i\hbar G_{nm}(t)=\delta(t). \tag{2.69}$$

With the help of appendix A.1, this gives

$$G_{nm}(t)=\frac{i}{\hbar}\Theta(t)\,e^{-i\omega_{nm}t-\Gamma_{nm}t}, \tag{2.70}$$

and

$$\boxed{\rho_{nm}(t)=G_{nm}(t)\otimes\left(E(t)\sum_l\left[\mu_{nl}\rho_{lm}(t)-\rho_{nl}(t)\mu_{lm}\right]\right).} \tag{2.71}$$

The result shows that the density matrix is a function of the Green's function, which can be interpreted as the impulsive response function of the system, as well as the electric field and the density matrix itself.

The Green's function $G_{nm}(t)$ as given by equation (2.70) is an exponentially decaying function with a decay rate $\Gamma_{nm}$, multiplied with a harmonic oscillation with frequency $\omega_{nm}$, the resonance frequency of the system.

With $G_{nm}(t)$ corresponding to the response function of the system, the Fourier transform $G_{nm}(\omega)$ will similarly correspond to the susceptibility $\chi(\omega)$. The Fourier transform of equation (2.70) is

$$\begin{aligned}G_{nm}(\omega)&=\frac{-1/\hbar}{\omega-\omega_{nm}+i\Gamma_{nm}}\\&=-\frac{1}{\hbar}\frac{\omega-\omega_{nm}-i\Gamma_{nm}}{(\omega-\omega_{nm})^2+\Gamma_{nm}^2}.\end{aligned} \tag{2.72}$$

The imaginary part of the susceptibility yields the absorption coefficient for the transition $|n\rangle\rightarrow|m\rangle$ in the system:

$$\alpha(\omega)\propto\frac{\Gamma_{nm}}{(\omega-\omega_{nm})^2+\Gamma_{nm}^2}. \tag{2.73}$$

This means the system will have a Lorentzian absorption profile for the $|n\rangle\rightarrow|m\rangle$ transition centered at $\omega_{nm}$ and width determined by the dephasing rate $\Gamma_{nm}$.

With the assumption that the electric field is small, we can perform a perturbation expansion of equation (2.71), writing

$$\rho(t)=\rho^{(1)}(t)+\rho^{(2)}(t)+\rho^{(3)}(t)+\ldots \tag{2.74}$$

where $\rho^{(p)}$ is of order $p$ in the electric field. Given the form of equation (2.71), the density matrix element of order $p+1$ is simply given as

$$\boxed{\rho_{nm}^{(p+1)}(t)=G_{nm}(t)\otimes\left(E(t)\sum_l\left[\mu_{nl}\rho_{lm}^{(p)}(t)-\rho_{nl}^{(p)}(t)\mu_{lm}\right]\right).} \tag{2.75}$$

This gives a means of computing iteratively the density matrix up to a given order in the electric field. In the following, we use double sided Feynman diagrams explained in appendix A.2 to represent equation (2.75) graphically.

### 2.3.1. Two-Level System

We begin by applying the above equations to a system with only two possible energy states, the ground state $|\mathrm{g}\rangle$ and the excited state $|\mathrm{e}\rangle$, as shown in figure 2.5.

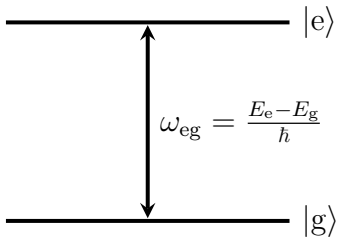


Figure 2.5.: Energy levels in the two-level system.

With the assumption that the system has a center of inversion, such that $\mu_{\mathrm{gg}}$ and $\mu_{\mathrm{ee}}$ are zero, the equations for the perturbation expansion of the density matrix elements will be given as

$$\rho_{\mathrm{eg}}^{(p+1)}(t) = G_{\mathrm{eg}}(t) \otimes \left( E(t) \left[ \mu_{\mathrm{eg}} \rho_{\mathrm{gg}}^{(p)}(t) - \rho_{\mathrm{ee}}^{(p)}(t) \mu_{\mathrm{eg}} \right] \right), \tag{2.76}$$

$$\rho_{\mathrm{ee}}^{(p+1)}(t) = G_{\mathrm{ee}}(t) \otimes \left( E(t) \left[ \mu_{\mathrm{eg}} \rho_{\mathrm{ge}}^{(p)}(t) - \rho_{\mathrm{eg}}^{(p)}(t) \mu_{\mathrm{ge}} \right] \right). \tag{2.77}$$

The total population has to be conserved so that

$$\rho_{\mathrm{gg}}^{(p)}(t) = -\rho_{\mathrm{ee}}^{(p)}(t), \qquad p > 0. \tag{2.78}$$

We further assume that the thermal energy is sufficiently small that only the ground state is populated with no field present. This determines the time independent, zeroth order:

$$\rho_{\mathrm{gg}}^{(0)} = 1, \tag{2.79}$$

$$\rho_{\mathrm{nm} \neq \mathrm{gg}}^{(0)} = 0. \tag{2.80}$$

It is easily seen that the population terms given by equation (2.76) will only have contributions of even order in the expansion, while coherences given by equation (2.77) only have contributions of odd order.

The first order coherence is given by

$$\begin{aligned} \rho_{\mathrm{eg}}^{(1)}(t) &= G_{\mathrm{eg}}(t) \otimes \left( E(t) \left[ \mu_{\mathrm{eg}} \rho_{\mathrm{gg}}^{(0)}(t) - \rho_{\mathrm{ee}}^{(0)}(t) \mu_{\mathrm{eg}} \right] \right) \\ &= \mu_{\mathrm{eg}} G_{\mathrm{eg}}(t) \otimes E(t), \end{aligned} \tag{2.81}$$

leading to the second order population

$$\begin{aligned} \rho_{\mathrm{ee}}^{(2)}(t) &= G_{\mathrm{ee}}(t) \otimes \left( E(t) \left[ \mu_{\mathrm{eg}} \rho_{\mathrm{ge}}^{(1)}(t) - \rho_{\mathrm{eg}}^{(1)}(t) \mu_{\mathrm{ge}} \right] \right) \\ &= -|\mu_{\mathrm{eg}}|^2 G_{\mathrm{ee}}(t) \otimes \left( E(t) \left[ (G_{\mathrm{eg}}(t) + G_{\mathrm{ge}}(t)) \otimes E(t) \right] \right). \end{aligned} \tag{2.82}$$

Using the identity $\rho^{(2)}_{gg}(t) + \rho^{(2)}_{ee}(t) = 0$, giving $\rho^{(2)}_{gg}(t) - \rho^{(2)}_{ee}(t) = -2\rho^{(2)}_{ee}(t)$, the third order coherence, given as

$$\rho^{(3)}_{eg}(t) = \mu_{eg} G_{eg}(t) \otimes \left( E(t) \left[ \rho^{(2)}_{gg}(t) - \rho^{(2)}_{ee}(t) \right] \right), \tag{2.83}$$

can be rewritten

$$\begin{aligned} \rho^{(3)}_{eg}(t) &= -2\mu_{eg} G_{eg}(t) \otimes \left( E(t) \left[ \rho^{(2)}_{ee}(t) \right] \right) \\ &= 2\mu_{eg} |\mu_{eg}|^2 G_{eg}(t) \otimes \left( E(t) \left[ G_{ee}(t) \otimes \left( E(t) \left[ (G_{eg}(t) + G_{ge}(t)) \otimes E(t) \right] \right) \right] \right). \end{aligned} \tag{2.84}$$

### 2.3.2. The Rotating Wave Approximation (RWA)

With a complex notation for the electric fields, $E(t) = (\mathcal{E}(t) + \mathcal{E}^*(t))/2$ inserted in the above equations, we end up with twice as many terms. In the rotating wave approximation (RWA) however, we only keep the terms close to resonance. For example, $G_{eg}(t) \otimes \mathcal{E}(t)$ is resonant, while $G_{eg}(t) \otimes \mathcal{E}^*(t)$ is not. This is also evident from evaluating the overlap of the functions in the frequency domain: $G_{eg}(\omega)\mathcal{E}(\omega)$ is much larger than $G_{eg}(\omega)\mathcal{E}^*(-\omega)$, thus giving a much larger contribution. Keeping only the resonant contributions, equation (2.84) becomes

$$\begin{aligned} \rho^{(3)}_{eg}(t) = &\frac{\mu_{eg}\mu_{ge}\mu_{eg}}{4} G_{eg}(t) \otimes \{ \mathcal{E}(t) \left[ G_{ee}(t) \otimes \right. \\ &\left. \left( \mathcal{E}^*(t) \left\{ G_{eg}(t) \otimes \mathcal{E}(t) \right\} + \mathcal{E}(t) \left\{ G_{ge}(t) \otimes \mathcal{E}^*(t) \right\} \right) \right] \}. \end{aligned} \tag{2.85}$$

### 2.3.3. Pump and Probe Fields

The total (complex) electric field is given as the sum of the pump and probe (test) fields:

$$\mathcal{E}(t) = \mathcal{E}_P(t) + \mathcal{E}_T(t). \tag{2.86}$$

The third order coherence is thus obtained by inserting this in equation (2.85). With an experimental set-up where only the signal in the direction of the probe field is measured however, only induced polarisation radiating a field in the same direction as the probe field will contribute to the signal. With fields given as

$$\mathcal{E}_P \propto e^{i\mathbf{k}_P \cdot \mathbf{r}}, \tag{2.87}$$

$$\mathcal{E}_T \propto e^{i\mathbf{k}_T \cdot \mathbf{r}}, \tag{2.88}$$

the part of the induced polarisation radiating a field in the $\mathbf{k}_T$ direction will include the three fields $\mathcal{E}_P(t)$, $\mathcal{E}^*_P(t)$ and $\mathcal{E}_T(t)$[1]. This gives the following three contributions to the third order coherence when only considering the $\mathbf{k}_T$ direction:

$$\begin{aligned} \rho^{(3,\mathrm{TPP})}_{eg}(t) = &\frac{\mu_{eg}\mu_{ge}\mu_{eg}}{4} G_{eg}(t) \otimes \{ \mathcal{E}_T(t) \left[ G_{ee}(t) \otimes \right. \\ &\left. \left( \mathcal{E}^*_P(t) \left\{ G_{eg}(t) \otimes \mathcal{E}_P(t) \right\} + \mathcal{E}_P(t) \left\{ G_{ge}(t) \otimes \mathcal{E}^*_P(t) \right\} \right) \right] \}, \end{aligned} \tag{2.89}$$

[1]The contribution from the term including the fields $\mathcal{E}_T(t)$, $\mathcal{E}^*_T(t)$ and $\mathcal{E}_T(t)$ will also have the right direction, but as the probe field is much weaker than the pump field, we ignore this term.

$$\rho_{\mathrm{eg}}^{(3,\mathrm{PTP})}(t) = \frac{\mu_{\mathrm{eg}}\mu_{\mathrm{ge}}\mu_{\mathrm{eg}}}{4} G_{\mathrm{eg}}(t) \otimes \{\mathcal{E}_{\mathrm{P}}(t)\,[G_{\mathrm{ee}}(t) \otimes (\mathcal{E}_{\mathrm{T}}(t)\,\{G_{\mathrm{ge}}(t) \otimes \mathcal{E}_{\mathrm{P}}^{*}(t)\})]\}\,, \tag{2.90}$$

$$\rho_{\mathrm{eg}}^{(3,\mathrm{PPT})}(t) = \frac{\mu_{\mathrm{eg}}\mu_{\mathrm{ge}}\mu_{\mathrm{eg}}}{4} G_{\mathrm{eg}}(t) \otimes \{\mathcal{E}_{\mathrm{P}}(t)\,[G_{\mathrm{ee}}(t) \otimes (\mathcal{E}_{\mathrm{P}}^{*}(t)\,\{G_{\mathrm{eg}}(t) \otimes \mathcal{E}_{\mathrm{T}}(t)\})]\}\,, \tag{2.91}$$

where the extra index (TPP etc.) denotes the time ordering of the fields. The three contributions correspond to the Feynman diagrams shown in figure 2.6 where the time ordering is easily recognized. We denote the three contributions the population term (TTP), polarization coupling term (PTP) and perturbed polarization term (PPT) [10].

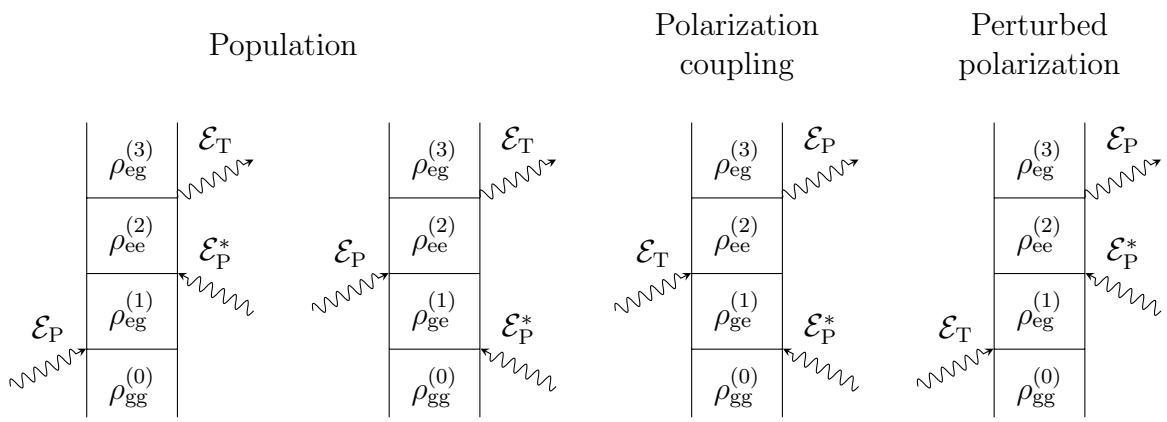


Figure 2.6.: Contributions to the pump-probe signal in a two-level system.

### 2.3.4. Pump-Probe Signal

The measured signal depends on the electric field radiated by the third order polarisation given by

$$P^{(3)}(t) = N\langle\mu^{(3)}(t)\rangle = N\,\mathrm{Tr}\{\mu\rho^{(3)}(t)\}. \tag{2.92}$$

In the two-level system, this becomes

$$P^{(3)}(t) = N(\mu_{\mathrm{ge}}\rho_{\mathrm{eg}}^{(3)}(t) + \mu_{\mathrm{eg}}\rho_{\mathrm{ge}}^{(3)}(t)) = N(\mu_{\mathrm{ge}}\rho_{\mathrm{eg}}^{(3)}(t) + \mathrm{c.c}) = 2N\mathrm{Re}\{\mu_{\mathrm{ge}}\rho_{\mathrm{eg}}^{(3)}(t)\}. \tag{2.93}$$

The third order complex polarization $\mathcal{P}^{(3)}(t)$ is thus given as

$$\boxed{\mathcal{P}^{(3)}(t) = 2N\mu_{\mathrm{ge}}\rho_{\mathrm{eg}}^{(3)}(t),} \tag{2.94}$$

in accordance with the usual definition

$$P^{(3)}(t) = \mathrm{Re}\{\mathcal{P}^{(3)}(t)\}. \tag{2.95}$$

By inserting equation (2.94) into equations (2.31) and (2.33) we get the integrated and spectrally resolved pump-probe signal respectively.

### 2.3.5. Comparison to the Classical Approach

In the case of instantaneous dephasing, $G_{\mathrm{eg}}(t) = i\delta(t)$, the medium investigated will be frequency independent in the spectrum of the pump and probe pulses. This broad absorption spectrum was one of the assumptions when deriving the classical signal in section 2.2.1. Mathematically, the contributions to the pump-probe signal given by equations (2.89) to (2.91) reduce to

$$\rho_{\mathrm{eg}}^{(3,\mathrm{TPP})}(t) = -\frac{\mu_{\mathrm{eg}}\mu_{\mathrm{ge}}\mu_{\mathrm{eg}}}{2}\mathcal{E}_{\mathrm{T}}(t)\left(G_{\mathrm{ee}}(t) \otimes |\mathcal{E}_{\mathrm{P}}(t)|^2\right), \tag{2.96}$$

$$\rho_{\mathrm{eg}}^{(3,\mathrm{PTP})}(t) = -\frac{\mu_{\mathrm{eg}}\mu_{\mathrm{ge}}\mu_{\mathrm{eg}}}{4}\mathcal{E}_{\mathrm{P}}(t)\big(G_{\mathrm{ee}}(t) \otimes \mathcal{E}_{\mathrm{P}}^{*}(t)\mathcal{E}_{\mathrm{T}}(t)\big), \tag{2.97}$$

and $\rho_{\mathrm{eg}}^{(3,\mathrm{PPT})}(t) = \rho_{\mathrm{eg}}^{(3,\mathrm{PTP})}(t)$ as there is no way of determining the ordering of the two "first" fields anymore. With equation (2.31) we get the signal from the two contributions

$$\Delta U(\tau)^{(\mathrm{TPP})} = \frac{n\omega_c L}{\epsilon_0 c}|\mu_{\mathrm{eg}}|^4 N \int_{-\infty}^{\infty} dt\, \mathrm{Im}\left\{|\mathcal{E}_{\mathrm{T}}(t)|^2\left(G_{\mathrm{ee}}(t) \otimes |\mathcal{E}_{\mathrm{P}}(t)|^2\right)\right\}, \tag{2.98}$$

$$\Delta U(\tau)^{(\mathrm{PTP+PPT})} = \frac{n\omega_c L}{\epsilon_0 c}|\mu_{\mathrm{eg}}|^4 N \int_{-\infty}^{\infty} dt\, \mathrm{Im}\left\{\mathcal{E}_{\mathrm{T}}(t)\mathcal{E}_{\mathrm{P}}^{*}(t)\big(G_{\mathrm{ee}}(t) \otimes \mathcal{E}_{\mathrm{P}}(t)\mathcal{E}_{\mathrm{T}}(t)^{*}\big)\right\}. \tag{2.99}$$

These two contributions are identical to the $\gamma(\tau)$ and $\beta(\tau)$ terms given in section 2.2.1 when we set $G_{\mathrm{ee}}(t)$ to be the third order on-resonance response function of the system. The population term (TPP) corresponds to the saturation term $\gamma(\tau)$, while the polarized coupling (PTP) and perturbed polarization (PPT) terms together give the coherent signal $\beta(\tau)$. Thus, in the case of instantaneous dephasing ($T_2 = 0$), the expressions for the pump-probe signal obtained through the density matrix approach are reduced to the classical result of section 2.2.1.

### 2.3.6. Three-Level System

In the two-level system, whatever leaves the high energy state has to enter the low energy state. This means the pump-probe signal after the initial rise always will decrease with increasing probe delay $\tau$, as the high energy level is depleted. To illustrate a case where the pump-probe signal may increase further after the initial rise, we introduce a third level, and denote the levels $|0\rangle$, $|1\rangle$ and $|2\rangle$. We choose the energy of $|2\rangle$ close to $|1\rangle$, such that $\omega_{21}$ is considerably smaller than $\omega_{10}$ and $\omega_{20}$, as shown in figure 2.7. By pumping $|3\rangle$ and allowing the population of $|3\rangle$ to relax to $|2\rangle$, probing $|2\rangle$ will give a rising pump-probe signal even after the initial increase.

We first present the equations for the third order density matrix elements, as in the two-level approach above, before introducing the extra relaxation between the highest energy levels. We will however make some assumptions to reduce the number of contributing terms: As explained in section 2.3.5, the coherent artifact arises from terms where the probe field precedes the pump pulse (PPT), or overlaps with the pump field (PTP). In section 2.2.1, we give examples on how to reduce the coherent artifact, so that the population term (TPP) is the main contribution to the pump-probe signal. We will

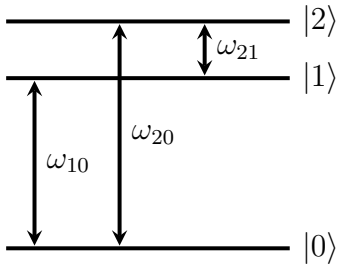


Figure 2.7.: Energy levels of the three-level system.

therefore only keep the population term in the following. We also limit ourselves to the case of a spectrally narrow pump. The pump can thus induce only one of the transition $|0\rangle \to |1\rangle$ or $|0\rangle \to |2\rangle$. The probe may however be spectrally broad, making it possible to probe both transition. In addition, the rotating wave approximation is applied.

By applying equation (2.75) to the three-level system, we get the equations governing the density matrix elements:

$$\rho_{10}^{(p+1)}(t) = G_{10}(t) \otimes \left( E(t) \left[ \mu_{10}\rho_{00}^{(p)}(t) - \rho_{11}^{(p)}(t)\mu_{10} + \mu_{12}\rho_{20}^{(p)}(t) - \rho_{12}^{(p)}(t)\mu_{20} \right] \right), \quad (2.100)$$

$$\rho_{20}^{(p+1)}(t) = G_{20}(t) \otimes \left( E(t) \left[ \mu_{20}\rho_{00}^{(p)}(t) + \mu_{21}\rho_{10}^{(p)}(t) - \rho_{21}^{(p)}(t)\mu_{10} - \rho_{22}^{(p)}(t)\mu_{20} \right] \right), \quad (2.101)$$

$$\rho_{21}^{(p+1)}(t) = G_{21}(t) \otimes \left( E(t) \left[ \mu_{20}\rho_{01}^{(p)}(t) - \rho_{20}^{(p)}(t)\mu_{01} + \mu_{21}\rho_{11}^{(p)}(t) - \rho_{22}^{(p)}(t)\mu_{21} \right] \right), \quad (2.102)$$

$$\rho_{11}^{(p+1)}(t) = G_{11}(t) \otimes \left( E(t) \left[ \mu_{10}\rho_{01}^{(p)}(t) - \rho_{10}^{(p)}(t)\mu_{01} + \mu_{12}\rho_{21}^{(p)}(t) - \rho_{12}^{(p)}(t)\mu_{21} \right] \right), \quad (2.103)$$

$$\rho_{22}^{(p+1)}(t) = G_{22}(t) \otimes \left( E(t) \left[ \mu_{20}\rho_{02}^{(p)}(t) - \rho_{20}^{(p)}(t)\mu_{02} + \mu_{21}\rho_{12}^{(p)}(t) - \rho_{21}^{(p)}(t)\mu_{12} \right] \right), \quad (2.104)$$

and, by choosing $\rho_{00}^{(0)} = 1$ as earlier,

$$\rho_{00}^{(p)}(t) = -\left[ \rho_{11}^{(p)}(t) + \rho_{22}^{(p)}(t) \right], \qquad p > 0, \quad (2.105)$$

since the total population is constant, giving

$$\mathrm{Tr}\left\{ \rho^{(p)}(t) \right\} = 0, \qquad p > 0. \quad (2.106)$$

We next evaluate the density matrix elements for increasing order $p$.

### Zeroth Order

We have already chosen the initial condition

$$\rho_{00}^{(0)} = 1, \quad (2.107)$$

which means

$$\rho_{nm\neq 00}^{(0)} = 0. \quad (2.108)$$

### First Order

Only two matrix elements are non-zero to first order:

$$\begin{aligned}\rho_{10}^{(1)}(t) &= G_{10}(t) \otimes \left( E(t) \left[ \mu_{10} \rho_{00}^{(0)}(t) \right] \right) \\ &= \mu_{10} G_{10}(t) \otimes E(t), \end{aligned} \tag{2.109}$$

$$\begin{aligned}\rho_{20}^{(1)}(t) &= G_{20}(t) \otimes \left( E(t) \left[ \mu_{20} \rho_{00}^{(p)}(t) \right] \right) \\ &= \mu_{20} G_{20}(t) \otimes E(t), \end{aligned} \tag{2.110}$$

while

$$\rho_{21}^{(1)}(t) = \rho_{11}^{(1)}(t) = \rho_{22}^{(1)}(t) = \rho_{00}^{(1)}(t) = 0. \tag{2.111}$$

### Second Order

To second order, the coherence terms are

$$\begin{aligned}\rho_{10}^{(2)}(t) &= G_{10}(t) \otimes \left( E(t) \left[ \mu_{12} \rho_{20}^{(1)}(t) \right] \right) \\ &= \mu_{12} \mu_{20} G_{10}(t) \otimes \left( E(t) \left[ G_{20}(t) \otimes E(t) \right] \right), \end{aligned} \tag{2.112}$$

$$\begin{aligned}\rho_{20}^{(2)}(t) &= G_{20}(t) \otimes \left( E(t) \left[ \mu_{21} \rho_{10}^{(1)}(t) \right] \right) \\ &= \mu_{21} \mu_{10} G_{20}(t) \otimes \left( E(t) \left[ G_{10}(t) \otimes E(t) \right] \right), \end{aligned} \tag{2.113}$$

$$\begin{aligned}\rho_{21}^{(2)}(t) &= G_{21}(t) \otimes \left( E(t) \left[ \mu_{20} \rho_{01}^{(1)}(t) - \rho_{20}^{(1)}(t) \mu_{01} \right] \right) \\ &= -\mu_{20} \mu_{01} G_{21}(t) \otimes \left( E(t) \left[ (G_{01}(t) + G_{20}(t)) \otimes E(t) \right] \right). \end{aligned} \tag{2.114}$$

These three terms require that the first two fields are able to induce two different transitions in the material. As we are limited to the case when the two first fields interacting with the system are the pump, which is only able to induce one transition, these transitions will not contribute to the pump-probe signal. The transitions are shown in figure 2.8.

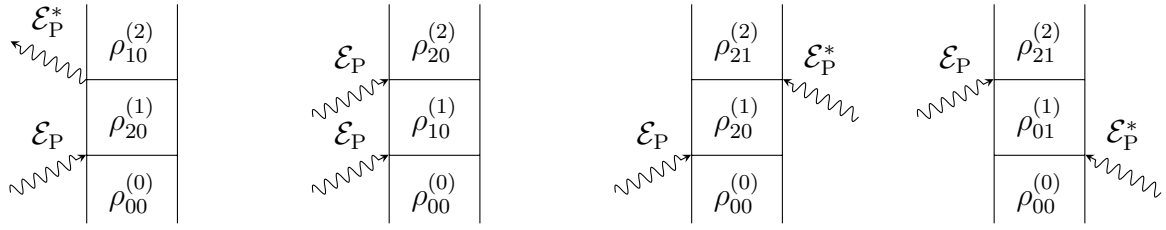


Figure 2.8.: Excitation of second order coherences in the three-level system.

Further, we have the population terms

$$\begin{aligned}\rho_{11}^{(2)}(t) &= G_{11}(t) \otimes \left( E(t) \left[ \mu_{10} \rho_{01}^{(1)}(t) - \rho_{10}^{(1)}(t) \mu_{01} \right] \right) \\ &= -|\mu_{10}|^2 G_{11}(t) \otimes \left( E(t) \left[ (G_{10}(t) + G_{01}(t)) \otimes E(t) \right] \right), \end{aligned} \tag{2.115}$$

$$\begin{aligned}\rho_{22}^{(2)}(t) &= G_{22}(t) \otimes \left( E(t) \left[ \mu_{20} \rho_{02}^{(1)}(t) - \rho_{20}^{(1)}(t) \mu_{02} \right] \right) \\ &= -|\mu_{20}|^2 G_{22}(t) \otimes \left( E(t) \left[ (G_{20}(t) + G_{02}(t)) \otimes E(t) \right] \right), \end{aligned} \tag{2.116}$$

shown in figure 2.9. These population terms require pumping of only one transition and thus contribute to the pump-probe signal.

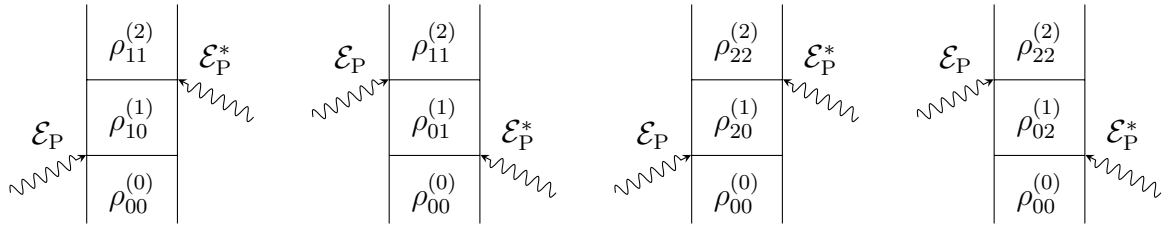


Figure 2.9.: Excitation of second order populations in the three-level system.

The transitions giving the third population term $\rho_{00}^{(2)}(t)$ are shown in figure 2.10. The simplest way to find this term however is through

$$\rho_{00}^{(2)}(t) = -\left[ \rho_{11}^{(2)}(t) + \rho_{22}^{(2)}(t) \right], \tag{2.117}$$

as the total population has to be conserved.

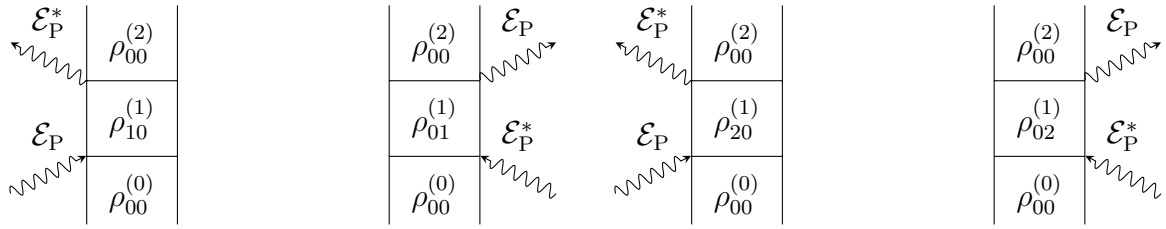


Figure 2.10.: Transitions contributing to $\rho_{00}^{(2)}(t)$ in the three-level system.

### Third Order

To third order, ignoring non-contributing second order coherences as explained above, we get

$$\rho_{10}^{(3)}(t) = G_{10}(t) \otimes \left( E(t) \left[ \mu_{10} \rho_{00}^{(2)}(t) - \rho_{11}^{(2)}(t) \mu_{10} \right] \right), \tag{2.118}$$

$$\rho_{20}^{(3)}(t) = G_{20}(t) \otimes \left( E(t) \left[ \mu_{20} \rho_{00}^{(2)}(t) - \rho_{22}^{(2)}(t) \mu_{20} \right] \right), \tag{2.119}$$

$$\rho_{21}^{(3)}(t) = G_{21}(t) \otimes \left( E(t) \left[ \mu_{21} \rho_{11}^{(2)}(t) - \rho_{22}^{(2)}(t) \mu_{21} \right] \right), \tag{2.120}$$

$$\rho_{11}^{(3)}(t) = \rho_{22}^{(3)}(t) = 0. \tag{2.121}$$

The transitions giving these coherences are shown in figure 2.11. With $\omega_{10}$ and $\omega_{20}$ much larger than $\omega_{21}$, we choose the spectrum of the probe such that it can induce both $|0\rangle \rightarrow |1\rangle$ and $|0\rangle \rightarrow |2\rangle$ transitions, but not the $|1\rangle \rightarrow |2\rangle$ transitions. We therefore ignore the term $\rho_{21}^{(3)}(t)$ in the following, as it does not contribute to the pump-probe signal.

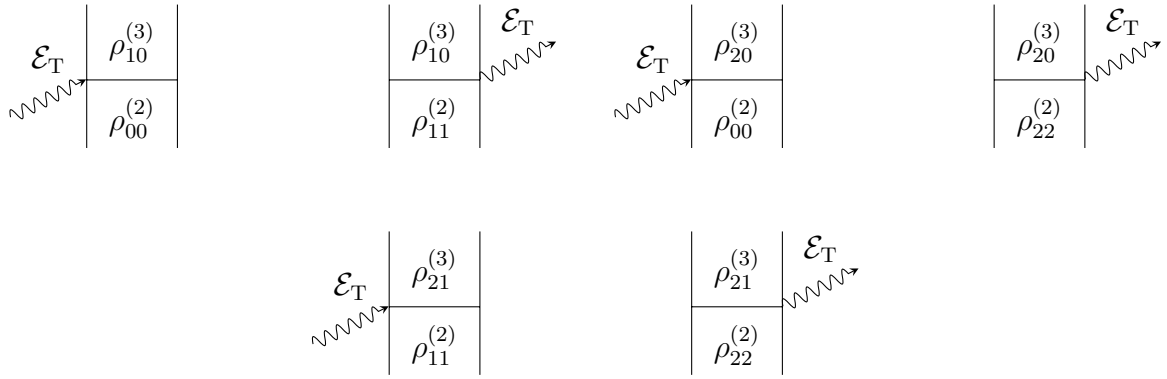


Figure 2.11.: Excitation of third order coherences in the three-level system

With the identity

$$\rho_{00}^{(2)}(t) + \rho_{11}^{(2)}(t) + \rho_{22}^{(2)}(t) = 0, \tag{2.122}$$

we rewrite equations (2.118) and (2.119) as

$$\begin{aligned}
\rho_{10}^{(3)}(t) &= -G_{10}(t) \otimes \left( E(t) \left[ 2\mu_{10} \rho_{11}^{(2)}(t) + \mu_{10} \rho_{22}^{(2)}(t) \right] \right) \\
&= \mu_{10} G_{10}(t) \otimes \Big( E(t) \Big[ 2|\mu_{10}|^2 G_{11}(t) \otimes \left( E(t) \left[ (G_{10}(t) + G_{01}(t)) \otimes E(t) \right] \right) \\
&\qquad + |\mu_{20}|^2 G_{22}(t) \otimes \left( E(t) \left[ (G_{20}(t) + G_{02}(t)) \otimes E(t) \right] \right) \Big] \Big),
\end{aligned} \tag{2.123}$$

$$\begin{aligned}
\rho_{20}^{(3)}(t) &= -G_{20}(t) \otimes \left( E(t) \left[ 2\mu_{20} \rho_{22}^{(2)}(t) + \mu_{20} \rho_{11}^{(2)}(t) \right] \right) \\
&= \mu_{20} G_{20}(t) \otimes \Big( E(t) \Big[ 2|\mu_{20}|^2 G_{22}(t) \otimes \left( E(t) \left[ (G_{20}(t) + G_{02}(t)) \otimes E(t) \right] \right) \\
&\qquad + |\mu_{10}|^2 G_{11}(t) \otimes \left( E(t) \left[ (G_{10}(t) + G_{01}(t)) \otimes E(t) \right] \right) \Big] \Big).
\end{aligned} \tag{2.124}$$

With the relation between polarization and the density matrix given in equation (2.92), only including contributing terms gives

$$\mathcal{P}^{(3)}(t) = 2N\left[\mu_{01}\rho_{10}^{(3)}(t) + \mu_{02}\rho_{20}^{(3)}(t)\right]. \tag{2.125}$$

The integrated and spectrally resolved pump-probe signals are then obtained by inserting for $\mathcal{P}^{(3)}(t)$ in equations (2.31) and (2.33).

### 2.3.7. Relaxation in a Three-Level System

The formalism presented this far assumes that that the exited states relaxes to the ground state only. This is valid in a two-level system as there is "nowhere else to go". With three levels however, there is a possibility for state $|2\rangle$ to relax to state $|1\rangle$. We next assume that both processes occur, and denote the fraction relaxing to $|0\rangle$ as $\eta_{20}$ and the fraction relaxing to $|1\rangle$ as $\eta_{21}$. The relaxation term given in the evolution equation for density matrix elements $\rho_{11}$ will then include relaxation from $\rho_{22}$ and is written[2]

$$\left.\frac{\partial\rho_{11}}{\partial t}\right|_{\text{relax}} = -\Gamma_{11}\rho_{11} + \eta_{21}\Gamma_{22}\rho_{22}, \tag{2.126}$$

assuming only the ground state is populated at thermal equilibrium. The evolution equation has to be rewritten as

$$-\left(\frac{\mathrm{d}}{\mathrm{d}t} + \Gamma_{11}\right) i\hbar\rho_{11}(t) = E(t)\sum_l \left[\mu_{1l}\rho_{l1}(t) + \rho_{1l}(t)\mu_{l1}\right] - i\hbar\eta_{21}\Gamma_{22}\rho_{22}(t), \tag{2.127}$$

giving

$$\rho_{11}(t) = G_{11}(t) \otimes \left(E(t)\sum_l \left[\mu_{1l}\rho_{l1}(t) + \rho_{1l}(t)\mu_{l1}\right] - i\hbar\eta_{21}\Gamma_{22}\rho_{22}(t)\right). \tag{2.128}$$

The expression for $\rho_{22}(t)$ is unaltered. We rewrite the perturbation expansion of $\rho_{11}^{(p)}(t)$ as

$$\rho_{11}^{(p+1)}(t) = G_{11}(t) \otimes \left(E(t)\sum_l \left[\mu_{1l}\rho_{l1}^{(p)}(t) + \rho_{1l}^{(p)}(t)\mu_{l1}\right] - i\hbar\eta_{21}\Gamma_{22}\rho_{22}^{(p+1)}(t)\right). \tag{2.129}$$

As $\rho_{22}^{(p)}(t) = 0$ for $p < 2$, the above expression deviates from the one previously presented first to second order in the perturbation expansion. Thus, to include relaxation in our model, we only have to substitute equation (2.115) with

$$\rho_{11}^{(2)}(t) = G_{11}(t) \otimes \left(E(t)\left[\mu_{10}\rho_{01}^{(1)}(t) - \rho_{10}^{(1)}(t)\mu_{01}\right] - i\hbar\eta_{21}\Gamma_{22}\rho_{22}^{(2)}(t)\right). \tag{2.130}$$

[2]Note that the evolution equation for $\rho_{22}$ is unaltered, and that we still write $\rho_{00} = 1 - \rho_{11} - \rho_{22}$.

## 2.4. Semiconductors

While all the cases given above treats optical transitions between discrete energy levels, the energy states of semiconductors are broadened, forming energy bands. Semiconductors are transparent to light with too little energy, but when the incoming photons exceed the "energy gap" of the semiconductor it can absorb a wide spectrum of frequencies. Figure 2.12a shows the energy band structure of the semiconductor gallium arsenide (GaAs), with energy given along the y-axis, and momentum or wave vector **k** along the x-axis for different directions in the crystal structure ($\Delta$,$\Lambda$, etc.). As photons carry very little momentum, optical transitions are drawn as vertical arrows in the diagram. Phonons on the other hand, carrying little energy, but more momentum, will induce horizontal or slanted horizontal transitions. The difference in energy between the highest peak of the valence (low energy) band and the conduction (high energy) band in GaAs is 1.43 eV [12], meaning GaAs will absorb light with shorter wavelength than about 867 nm, bringing it into a photoexcited state. As the peak of the valence band and valley of the conduction band are at the same **k**-vector $\Gamma$, the material is known as having a direct band gap, meaning an optical transition will directly excite the material. In an indirect band gap semiconductor such as silicon (Si), excitation of the material with energy slightly above the band gap requires a phonon interaction as well as an optical transition for the electron to "reach" the lowest valley of the conduction band. The band structure of Si is given in figure 2.12b.

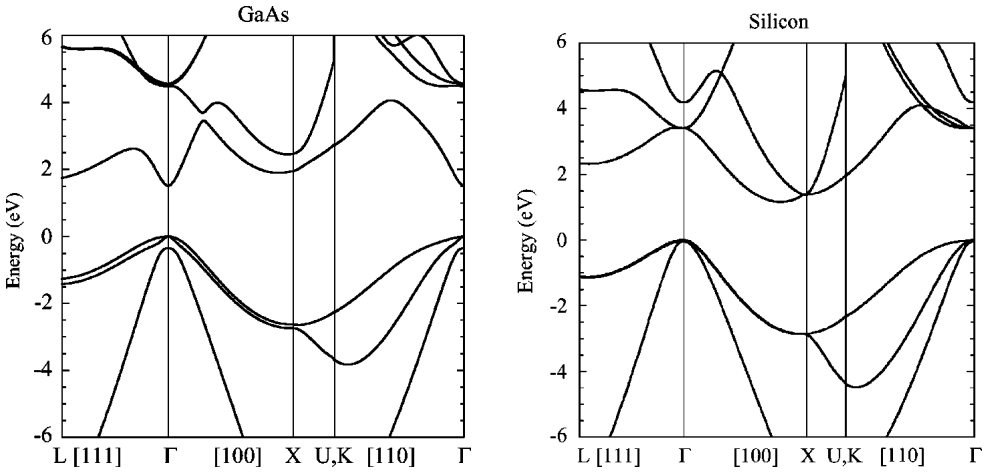


(a) Gallium Arsenide (GaAs). (b) Silicon (Si).

Figure 2.12.: Semiconductor band diagrams [13].

With this in mind, there will be some inherent differences in the absorption dynamics between the semiconductor and the discrete energy level systems presented so far. When exciting a semiconductor, electron transitions will occur vertically in the band diagram at the **k**-vector value(s) where the band gap match the energy of the excitation energy. The result is a great range of absorption frequencies as opposed to the narrow, symmetrical absorption of the discrete levels. This will render many of the equations presented so far inadequate for a semiconductor, as they have been derived assuming discrete levels. We

will however work around this with an alternative model for the absorption mechanics in semiconductors.

Another effect introduced with the band diagrams is the ability for carriers to re-distribute through electron-electron and phonon-electron scattering. Through electron-electron scattering, the initially excited "hot carriers" thermalize rapidly to a broader carrier distribution in the conduction band. At a longer time scale, the excited carrier distribution will cool through phonon-electron scattering. As phonons carry much less energy than electrons ($k_{\mathrm{B}}T \approx 0.024$ eV) carrier cooling is a slower process. On the other hand, phonons can have a considerable momentum, giving large horizontal transitions in the band-diagram, allowing scattering of the electrons into satellite valleys, illustrated by horizontal arrows in figure 2.13.

In e.g. GaAs, there is more than one valence band, as seen in figure 2.12a. When pumping with high enough energy, this results in several possible optical transitions as shown in figure 2.13. Electrons excited from the light hole (lh) and heavy (hh) hole bands, will therefore be excited to a much higher energy state in the conduction band than electrons excited from the split-off (so) hole band. Multiple hole bands will also affect the probing of the sample, as more than one transition is probed when the energy of the probe is high enough to couple the split-off band and conduction band.

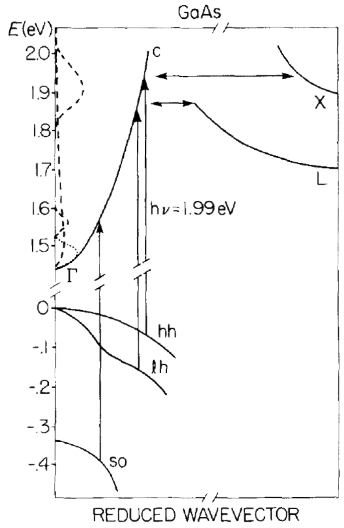


Figure 2.13.: Optical transitions and phonon scattering in GaAs pumped at 1.99 eV [14].

## 2.4.1. Experimental GaAs Pump-Probe Data

Figure 2.14 shows the result of a spectrally resolved pump-probe experiment of GaAs performed by Schoenlein et.al. [15, 16]. In the experiment, the sample was pumped by a laser pulse at 1.99 eV and probed with a continuum pulse. The probe energy as well as the change in transmission $\Delta T/T$ is given for each of the normalized pump-probe curves.

The original article explains how the initial peak visible for certain probe energies in the data originates from a fast relaxation process. Experiments with chirped pulses and

pulse polarization dependence of the peak, as well as different pulse durations concludes that the peak is not a coherent artifact.

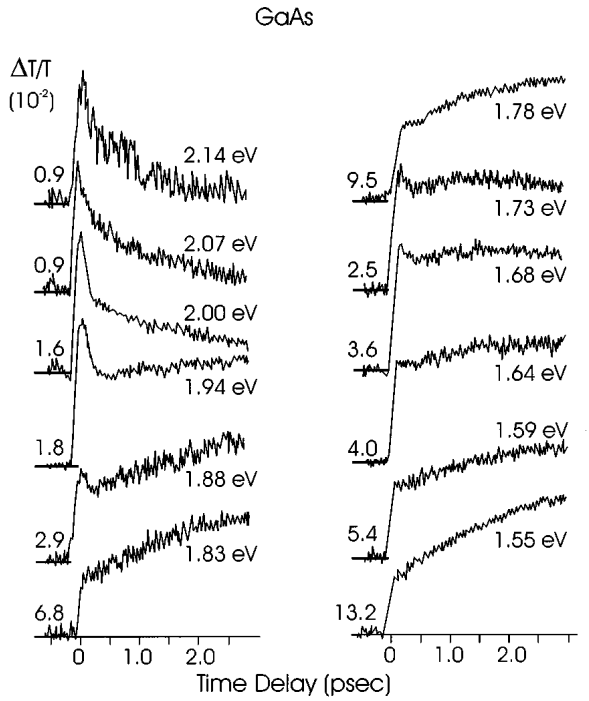


Figure 2.14.: Spectrally resolved pump-probe data for GaAs pumped at 1.99 eV [15, 16, 17].

The article authors assign the rapidly decaying peak at energies close to the pump energy to fast thermalization through electron-electron scattering. The fast initial rise at other energies is also explained by electrons redistributing in the conduction band through thermalization.

For longer probe delay times, the signal is governed by carrier cooling in the conduction band through phonon scattering. The carrier distribution moves towards lower energy, increasing the differential transmission signal for probe energies below the pump energy while decreasing the signal for probe energies exceeding the pump energy. For probe energies below 1.78 eV however, the energy of the probe is no longer sufficient to probe the split-off to conduction band transition, giving one less contribution to the signal. The remaining contributions come from probing the transition from the light and heavy hole bands to the conduction band, close to the energy of the initial population excited from the split-of band. This gives a quite constant transmission signal, with a small initial peak due to the thermalization of this initial population. For even lower probe energies, the transmission signal again increases for long probe delays.

Scattering to the satellite valleys may contribute to an increase in the signal, as the carriers return from the valleys on a picosecond time scale. It is however not easy to determine the size of this contribution from the pump-probe data presented.

## 2.5. Modelling the Pump-Probe Signal in Semiconductors

Because of the energy bands of semiconductors as opposed to the discrete energy levels in the density matrix approach, a different formalism should be applied to explain results from semiconductor experiments. A thorough numerical study by Bailey et al. [18] gives an exceptionally good fit to the experimental data from Schoenlein et al. presented above. They apply a Monte Carlo method for modelling electron and hole dynamics and use a 30 band $\mathbf{k} \cdot \mathbf{p}$ method to determine the energy states and density of states of the system.

We wish however to present a simpler approach to explain the main characteristics of the GaAs results. The model presented uses a naive approach to the dynamics in the pump-probe experiment. The interaction between field and population is however similar to the basic idea in the article by Bailey et al.

We let the population $N(\omega)_{t_n}$ at time $t_n$ be affected by the pump pulse $E_{\mathrm{P}}(\omega)_{t_n}$ and the previous population $N(\omega)_{t_{n-1}}$through

$$N(\omega)_{t_n} = |E_{\mathrm{P}}(\omega)_{t_n}|^2 \cdot \alpha(\omega) + (1 - r_{\mathrm{decay}}) \cdot N(\omega)_{t_{n-1}}, \tag{2.131}$$

where $r_{\mathrm{decay}}$ is the decay rate of the population, and $\alpha(\omega)$ is the absorption spectrum of the system.

Next, we assume that the absorption of a test pulse $E_{\mathrm{T}}$ incident on the sample is directly related to the excited population $N(\omega)$[3]. The excited population acts to reduce the absorption, resulting in a signal of increased differential transmission proportional to the excited population and the absorption spectrum. We write this numerically as

$$\Delta T(\omega;\tau)_{t_n} = |E_{\mathrm{T}}(\omega;\tau)_{t_n}|^2 \cdot \alpha(\omega) \cdot N(\omega)_{t_n}, \tag{2.132}$$

or, to model an experiment with a slow, time integrating detector

$$\Delta T(\omega;\tau) = \sum_{t_n} |E_{\mathrm{T}}(\omega;\tau)_{t_n}|^2 \cdot \alpha(\omega) \cdot N(\omega)_{t_n}. \tag{2.133}$$

We will next show how this model is related to the density matrix approach.

### 2.5.1. Comparison to the Density Matrix Approach

The analytical equivalent to equation (2.131) is the differential equation

$$\frac{\partial N(\omega,t)}{\partial t} = |E_{\mathrm{P}}(\omega,t)|^2 \cdot \alpha(\omega) - r_{\mathrm{decay}} \cdot N(\omega,t). \tag{2.134}$$

We rewrite this as

$$\left(\frac{\partial}{\partial t} + r\right) N(\omega,t) = |E_{\mathrm{P}}(\omega,t)|^2 \cdot \alpha(\omega), \tag{2.135}$$

and use appendix A.1 to solve the ODE. This gives

$$N(\omega,t) = G(t) \otimes |E_{\mathrm{P}}(\omega,t)|^2 \cdot \alpha(\omega), \tag{2.136}$$

[3]Or more correctly the population difference between the ground and excited state.

where we have defined the Green's function $G(t)$ as

$$G(t) = \Theta(t)e^{-rt}, \tag{2.137}$$

and $\Theta(t)$ is the Heaviside step function. To separate out the time and frequency we denote the frequency distribution of the field as $g_{\mathrm{P}}(\omega)$ and the time dependency of the field as $f_{\mathrm{P}}(t)$ to give

$$N(\omega, t) = G(t) \otimes f_{\mathrm{P}}(t)^2 \cdot \alpha(\omega) \cdot g_{\mathrm{P}}(\omega)^2. \tag{2.138}$$

In the case of a transform limited Gaussian pump pulse, both $g_{\mathrm{P}}(\omega)$ and $f_{\mathrm{P}}(t)$ are Gaussian functions. To verify the model, we will show how it relates to the results for a two-level system from section 2.3.

From section 2.3.3, we have that the population in the exited state for the case where the pump pulse proceeds the probe is given as

$$\rho_{\mathrm{ee}}^{(2)}(t) \propto G_{\mathrm{ee}}(t) \otimes \Big( \mathcal{E}_{\mathrm{P}}^*(t) \left\{ G_{\mathrm{eg}}(t) \otimes \mathcal{E}_{\mathrm{P}}(t) \right\} + \mathcal{E}_{\mathrm{P}}(t) \left\{ G_{\mathrm{ge}}(t) \otimes \mathcal{E}_{\mathrm{P}}^*(t) \right\} \Big). \tag{2.139}$$

This expression does not tell us the energy distribution of the population, other than that it is close to the energy of the exited state. We know however, given the response (Green's) functions treated earlier, that the absorption spectrum $\alpha(\omega)$ of the excited state is a Lorentzian function

$$\alpha(\omega) \propto \frac{T_2}{T_2^2(\omega - \omega_{\mathrm{eg}})^2 + 1}, \tag{2.140}$$

centered at the resonance $\omega_{\mathrm{eg}}$ and with peak width determined by the dephasing time $T_2$. In the case of a short dephasing time, the system will have a broad absorption spectrum.

The equation for $N(\omega, t)$ presented above, gives the frequency distribution explicitly. We integrate out the frequency dependence to be able to compare it to the expression for the density matrix element, obtaining

$$N(t) = G(t) \otimes f_{\mathrm{P}}(t)^2 \cdot C_{\mathrm{P}}^{\omega}, \tag{2.141}$$

where

$$C_{\mathrm{P}}^{\omega} = \int d\omega \, \alpha(\omega) g_{\mathrm{P}}(\omega)^2. \tag{2.142}$$

When investigating a system with a broad absorption spectrum $\alpha(\omega)$, we can treat the frequency distribution of the pump pulse $g_{\mathrm{P}}(\omega)^2$ as a delta function $\delta(\omega - \omega_{\mathrm{P}})$, and the above expression reduces to

$$C_{\mathrm{P}}^{\omega} = \int d\omega \, \alpha(\omega)\delta(\omega - \omega_{\mathrm{P}}) = \alpha(\omega_{\mathrm{P}}) = \frac{T_2}{T_2^2(\omega_{\mathrm{P}} - \omega_{\mathrm{eg}})^2 + 1}. \tag{2.143}$$

We will now show how to regain the expression for the population $N(t)$ from the expression for the density matrix element $\rho_{\mathrm{ee}}^{(2)}(t)$ given in (2.139):

$$\begin{aligned} \mathcal{E}_{\mathrm{P}}^*(t) \left\{ G_{\mathrm{eg}}(t) \otimes \mathcal{E}_{\mathrm{P}}(t) \right\} &= f_{\mathrm{P}}(t) e^{i\omega_{\mathrm{P}} t} \int \mathrm{d}t' \; \Theta(t') e^{-i\omega_{\mathrm{eg}} t'} e^{-t'/T_2} \cdot f_{\mathrm{P}}(t - t') e^{-i\omega_{\mathrm{P}}(t - t')} \\ &= f_{\mathrm{P}}(t) \int \mathrm{d}t' \; \Theta(t') e^{-i\omega_{\mathrm{eg}} t'} e^{-t'/T_2} \cdot f_{\mathrm{P}}(t - t') e^{i\omega_{\mathrm{P}}(t')}. \end{aligned} \tag{2.144}$$

With a short dephasing time $T_2$ compared to the length of the pulse, the integral will only depend on small values of $t'$ and we will have $f_{\mathrm{P}}(t-t') \approx f_{\mathrm{P}}(t)$. With $\Omega_{\mathrm{P}} = \omega_{\mathrm{P}} - \omega_{\mathrm{eg}}$ as the offset frequency, we get

$$\begin{aligned}\mathcal{E}_{\mathrm{P}}^{*}(t)\left\{G_{\mathrm{eg}}(t) \otimes \mathcal{E}_{\mathrm{P}}(t)\right\} &= f_{\mathrm{P}}(t)^2 \int_0^{\infty} \mathrm{d}t'\ e^{(i\Omega_{\mathrm{P}} - 1/T_2)t'} \\ &= f_{\mathrm{P}}(t)^2 \cdot \frac{1}{1/T_2 - i\Omega_{\mathrm{P}}} \\ &= f_{\mathrm{P}}(t)^2 \cdot T_2 \frac{1 + iT_2\Omega_{\mathrm{P}}}{1 + T_2^2\Omega_{\mathrm{P}}^2}. \end{aligned} \tag{2.145}$$

Similarly, we get

$$\mathcal{E}_{\mathrm{P}}(t)\left\{G_{\mathrm{ge}}(t) \otimes \mathcal{E}_{\mathrm{P}}^{*}(t)\right\} = f_{\mathrm{P}}(t)^2 \cdot T_2 \frac{1 - iT_2\Omega_{\mathrm{P}}}{1 + T_2^2\Omega_{\mathrm{P}}^2}, \tag{2.146}$$

so that

$$\rho_{\mathrm{ee}}^{(2)}(t) \propto G_{\mathrm{ee}}(t) \otimes f_{\mathrm{P}}(t)^2 \cdot \frac{T_2}{1 + T_2^2\Omega_{\mathrm{P}}^2}, \tag{2.147}$$

where we recognize the term

$$\frac{T_2}{1 + T_2^2\Omega_{\mathrm{P}}^2} = C_{\mathrm{P}}^{\omega} \tag{2.148}$$

from above. With $G_{\mathrm{ee}}(t) = G(t)$ we get

$$N(t) = \rho_{\mathrm{ee}}^{(2)}(t), \tag{2.149}$$

and

$$N(\omega, t) = \frac{\alpha(\omega) \cdot g_{\mathrm{P}}(\omega)^2}{C_{\mathrm{P}}^{\omega}} \rho_{\mathrm{ee}}^{(2)}(t), \tag{2.150}$$

which establishes the relation between $N(\omega, t)$ and $\rho_{\mathrm{ee}}^{(2)}(t)$.

The analytical counterpart of equation (2.133) is

$$\begin{aligned}\Delta T(\tau) &= \int_{-\infty}^{\infty} |E_{\mathrm{T}}(\omega, t; \tau)|^2 \cdot \alpha(\omega) \cdot N(\omega, t) dt \\ &= \int_{-\infty}^{\infty} f_{\mathrm{T}}(t; \tau)^2 \cdot g_{\mathrm{T}}(\omega)^2 \cdot \alpha(\omega) \cdot \frac{1}{C_{\mathrm{P}}^{\omega}} \alpha(\omega) \cdot g_{\mathrm{P}}(\omega)^2 \rho_{\mathrm{ee}}^{(2)}(t) dt \\ &= \frac{1}{C_{\mathrm{P}}^{\omega}} g_{\mathrm{P}}(\omega)^2 \cdot \alpha(\omega)^2 \cdot g_{\mathrm{T}}(\omega)^2 \int_{-\infty}^{\infty} f_{\mathrm{T}}(t; \tau)^2 \cdot \rho_{\mathrm{ee}}^{(2)}(t) dt, \end{aligned} \tag{2.151}$$

where we have inserted (2.150) for $N(\omega, t)$, $f_{\mathrm{T}}(t; \tau)$ is the time envelope of the test pulse, and $g_{\mathrm{T}}(\omega)$ is the frequency distribution. $\tau$ is the delay of the probe (test) pulse with respect to the pump. By choosing a broad distribution $g_{\mathrm{T}}(\omega)$, we can model probing with a spectral continuum, which in turn can give a spectrally resolved result. To simplify the math however, we will choose $g_{\mathrm{T}}(\omega) = g_{\mathrm{P}}(\omega)$, which represents a degenerate experiment where the pump and probe pulses are identical.

We integrate over all frequencies by assuming $g_{\mathrm{P}}(\omega)$ and $g_{\mathrm{T}}(\omega)$ as delta pulses as before, to obtain

$$\begin{aligned}\Delta T(\tau) &= \frac{1}{C_{\mathrm{P}}^{\omega}} \int_{-\infty}^{\infty} \alpha(\omega)^2 \delta(\omega - \omega_{\mathrm{P}}) \delta(\omega - \omega_{\mathrm{T}}) d\omega \int_{-\infty}^{\infty} f_{\mathrm{T}}(t;\tau)^2 \cdot \rho_{\mathrm{ee}}^{(2)}(t) dt \\ &= \frac{1}{C_{\mathrm{P}}^{\omega}} \cdot \alpha(\omega_{\mathrm{P/T}})^2 \int_{-\infty}^{\infty} f_{\mathrm{T}}(t;\tau)^2 \cdot \rho_{\mathrm{ee}}^{(2)}(t) dt \\ &= C_{\mathrm{T}}^{\omega} \int_{-\infty}^{\infty} f_{\mathrm{T}}(t;\tau)^2 \cdot \rho_{\mathrm{ee}}^{(2)}(t) dt, \end{aligned} \tag{2.152}$$

when $\omega_{\mathrm{P}} = \omega_{\mathrm{T}}$.

The spectrally integrated signal is given in section 2.1.2 as

$$\begin{aligned}\Delta U(\tau) &\propto \int_{-\infty}^{\infty} dt \mathrm{Im}\Big\{ \mathcal{E}_{\mathrm{T}}(t) \mathcal{P}^{(3)*}(t) \Big\} \\ &\propto \int_{-\infty}^{\infty} dt \mathrm{Im}\Big\{ \mathcal{E}_{\mathrm{T}}(t) \left[ G_{\mathrm{eg}}^{*}(t) \otimes \left\{ \mathcal{E}_{\mathrm{T}}^{*}(t) \rho_{\mathrm{ee}}^{(2)}(t) \right\} \right] \Big\}. \end{aligned} \tag{2.153}$$

As above, we evaluate the integrand in the case of rapid dephasing:

$$\begin{aligned}\mathcal{E}_{\mathrm{T}}(t) \left[ G_{\mathrm{eg}}^{*}(t) \otimes \left\{ \mathcal{E}_{\mathrm{T}}^{*}(t) \rho_{\mathrm{ee}}^{(2)}(t) \right\} \right] &= - f_{\mathrm{T}}(t) e^{-i\omega_{\mathrm{T}} t} \int \mathrm{d}t' \ \Theta(t') e^{i\omega_{\mathrm{eg}} t'} e^{-t'/T_2} \cdot f_{\mathrm{T}}(t - t') \rho_{\mathrm{ee}}^{(2)}(t) \\ &\approx - f_{\mathrm{T}}(t)^2 \rho_{\mathrm{ee}}^{(2)}(t) \int_0^{\infty} \mathrm{d}t' \ e^{-i\Omega_{\mathrm{T}} t'} e^{-t'/T_2} \\ &= - f_{\mathrm{T}}(t)^2 \rho_{\mathrm{ee}}^{(2)}(t) \cdot T_2 \frac{1 - iT_2\Omega_{\mathrm{T}}}{1 + T_2^2 \Omega_{\mathrm{T}}^2}, \end{aligned} \tag{2.154}$$

where we have assumed that both $f_{\mathrm{T}}(t - t')$ and $\rho_{\mathrm{ee}}^{(2)}(t - t')$ are almost constant in the short time interval $t'$ contributing to the integral because of the limiting term $e^{-t'/T_2}$. Combining (2.153) and (2.154), the spectrally integrated signal is given as

$$\Delta U(\tau) \propto C_{\mathrm{T}}^{\omega} \int_{-\infty}^{\infty} f_{\mathrm{T}}(t;\tau)^2 \rho_{\mathrm{ee}}^{(2)}(t), \tag{2.155}$$

where

$$C_{\mathrm{T}}^{\omega} = \frac{T_2}{1 + T_2^2 \Omega_{\mathrm{T}}^2}. \tag{2.156}$$

Comparing equation (2.155) with (2.152), we see that the model reproduces the results of section 2.3 for a two-level system with Lorentzian absorption, when the dephasing time is short compared to the pulse width, and the pulse is spectrally narrow compared to the absorption spectrum of the system. The model does not however include the contributions to the pump-probe signal where the probe precedes the pump pulse. Thus no coherent artifact will be present in the results obtained with this model.

### 2.5.2. Including Scattering Effects in the Semiconductor Model

The model does only reproduce the density matrix result at certain conditions. The validity of the model may therefore be questionable when choosing other conditions. The strength of this model is however that the absorption spectrum of the system can be chosen as any spectrally broad function and is not limited to the Lorentzian function resulting from the approach in section 2.3. The absorption spectrum can therefore be chosen to mimic that of a semiconductor, with an abrupt absorption edge and a broad absorption spectrum. Furthermore, more contributions can easily be added to the time evolution of the population $N(\omega)$, making it possible to include more effects in the model such as phonon scattering.

When modelling the transmitted signal in a semiconductor, the hole population in the valence band(s) is just as important as the electron population in the conduction band(s). We should therefore rather use

$$\Delta N(\omega)_{t_n} = N_{\mathrm{e}}(\omega)_{t_n} + N_{\mathrm{h}}(\omega)_{t_n}, \tag{2.157}$$

instead of just $N(\omega)$ in the expressions above. $N_{\mathrm{e}}$ and $N_{\mathrm{h}}$ are the electron and hole population respectively. We see from the part of the band diagram for GaAs in figure 2.13 that the hole bands are significantly less steep than the conduction band, making the low energy phonons much more effective scatterers in the valence band. To simplify, we will therefore assume a flat hole band with very rapid scattering as shown in figure 2.15. This means the hole energy is equal for every $\mathbf{k}$-value, and holes are equally likely to scatter to both higher and lower values of $\mathbf{k}$. As all holes have the same energy, we let $N_{\mathrm{h}}(\omega)$ refer to the population at a certain $\mathbf{k}$-vector corresponding to the energy $\omega$ of an electron in the conduction band with that particular $\mathbf{k}$-vector.

In the conduction band, we assume the electron population to cool through phonon scattering. This will however happen at a much slower rate than the scattering in the hole band because of the steepness of the conduction band, making the low energetic phonons less effective scatterers. All scattering processes are still sufficiently fast that optical electron-hole recombination can be neglected for the time delays investigated ($\sim$ps). Rather than equation (2.131), we use

$$N(\omega)_{t_n} = |E_{\mathrm{P}}(\omega)_{t_n}|^2 \cdot \alpha(\omega) + S\left[N(\omega)_{t_{n-1}}\right], \tag{2.158}$$

where $S$ is some appropriately chosen function representing scattering. In the conduction band, we model scattering as

$$N_{\mathrm{e}}(\omega)_{t_n} = |E_{\mathrm{P}}(\omega)_{t_n}|^2 \cdot \alpha(\omega) + N_{\mathrm{e}}(\omega + s_{\mathrm{e}})_{t_{n-1}}. \tag{2.159}$$

The population is still pumped by the incoming field (arrow 1, figure 2.15), but rather than decaying to the ground state, it shifts to lower values of $\omega$ with time at a rate $s_{\mathrm{e}}$ (arrow 3, figure 2.15).

In the hole band we model the scattering as

$$N_{\mathrm{h}}(\omega)_{t_n} = |E_{\mathrm{P}}(\omega)_{t_n}|^2 \cdot \alpha(\omega) + (1 - s_{\mathrm{h}}) N_{\mathrm{h}}(\omega)_{t_{n-1}} + s_{\mathrm{h}} \int N_{\mathrm{h}}(\omega)_{t_{n-1}} d\omega \cdot \frac{N_{\mathrm{h}}^{\mathrm{eq}}(\omega)}{\int N_{\mathrm{h}}^{\mathrm{eq}}(\omega) d\omega}. \tag{2.160}$$

The hole population is also pumped by the incoming field. With time, the population redistributes to become proportional to an equilibrium distribution $N_{\mathrm{h}}^{\mathrm{eq}}(\omega)$ at a rate $s_{\mathrm{h}}$ (arrows 2, figure 2.15).

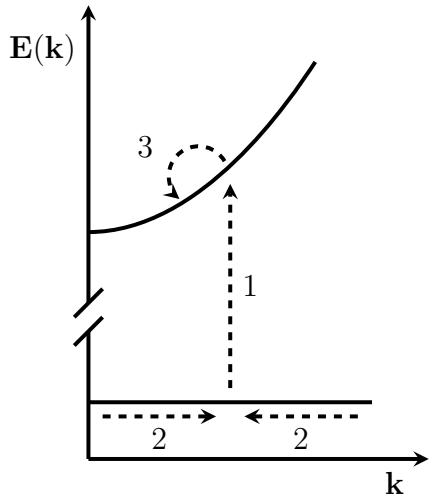


Figure 2.15.: Electron/hole transitions in the simplified model: The electrons are first pumped from the valence to electron band(1). Because of the flat valence band, the holes redistribute quickly(2) while the electrons in the conduction band cool at a slower rate(3).

# 3. Results and Discussion

All results are numerical simulations obtained from Matlab scripts based on the results from the theory section.

## 3.1. Classical Approach

The pump-probe signal resulting from the classical approach as given in equations (2.49) and (2.50) is evaluated numerically for a degenerate pump-probe experiment with Gaussian pulses of duration $\tau_E$. A typical exponentially decaying response function

$$A^{(3)}(t) = \Theta(t)e^{-t/\tau_{\mathrm{R}}} \tag{3.1}$$

is chosen, where $\Theta(t)$ is the step function. The limiting cases $\tau_{\mathrm{R}} = 0$ and $\tau_{\mathrm{R}} = \infty$ give the delta function and step function treated analytically in section 2.2.1. Figure 3.1 shows the normalized result for some values of the characteristic response decay time of the system $\tau_{\mathrm{R}}$. This clearly shows that when the material response time is on the same time scale as the pulse duration, the shape of the resulting pump-probe signal is governed by the pulse rather than by the system investigated.

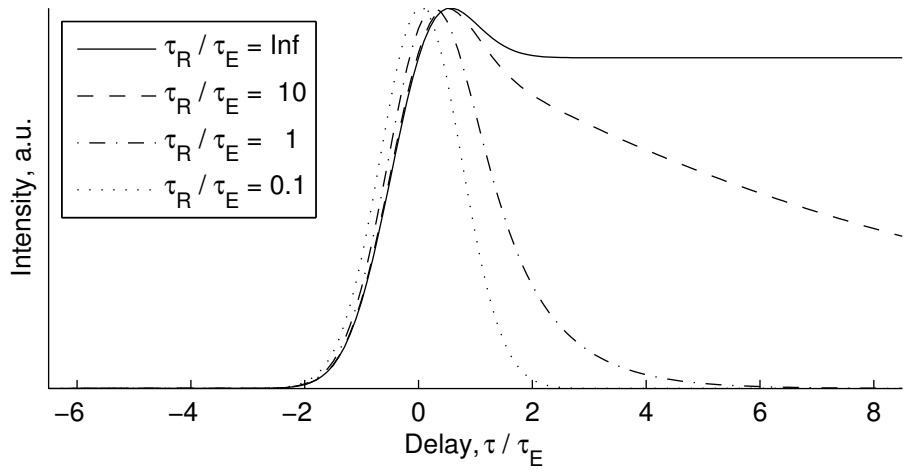


Figure 3.1.: Normalized pump-probe signal for different response function characteristic decay times $\tau_{\mathrm{R}}$ probed width Gaussian pulses of duration $\tau_E$.

## 3.2. Density Matrix Approach - Two-Level system

We use the results from section 2.3 to simulate the pump-probe signal for a two-level system. Figure 3.2 shows the result when pumping and probing with Gaussian pulses at the resonance frequency of the system. We have introduced a finite dephasing time $T_2 = 20\tau_E$.

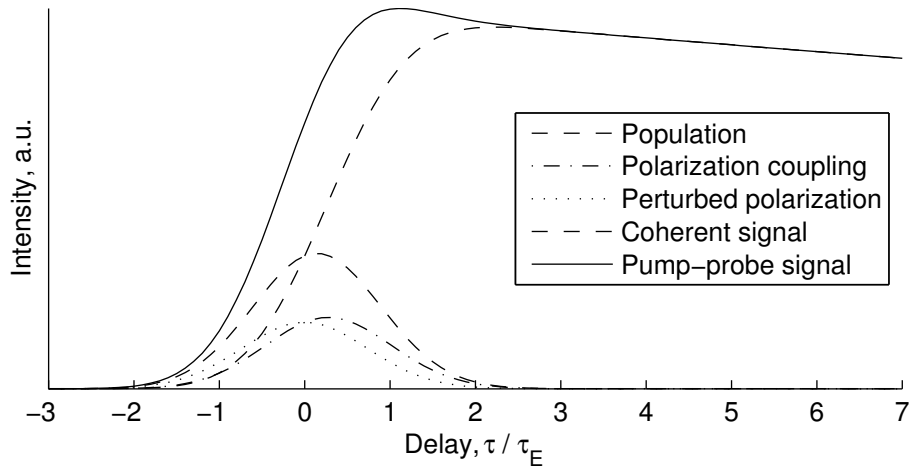


Figure 3.2.: Contributions to the integrated on-resonance degenerate pump-probe signal for a system with dephasing time $T_2 = 20\tau_E$.

Comparing with figure 2.2, it is clear that the introduction of finite dephasing changes the contributions to the signal. While the perturbed polarization contribution is symmetric around zero delay time, a shift towards longer delay has been introduced to the polarization coupling contribution. As the coherent signal is the sum of these terms as explained above, the coherent signal will also shift towards longer delay. Furthermore, the figure shows a positive shift in the population term, which no longer has its half-maximum value at $\tau = 0$. According to Chachisvillis et al. [19], these shifts are due to the symmetry of the time ordering of the fields. The time ordering of all pump and test fields involved in the perturbed polarization is TPPT, while for the population and polarization coupling terms it is TTPP and TPTP respectively (with the rightmost letter giving the first field and so on).

What is also evident from comparing with figure 2.2 is the reduced contribution of the coherent signal compared to the population term. While the coherent term peaked at half the maximum value of the population term in the case of instantaneous dephasing, it is slightly smaller with the chosen finite dephasing time. At zero delay however, the coherent term equals the population term, as always.

None of the terms in the integrated pump-probe signal contribute for large negative delay times, as one would expect. When looking at the spectrally resolved signal in figure 3.3 however, there is a considerable signal at some frequencies for negative delay times. We still pump the system with a Gaussian pulse centered at the resonance frequency ($\omega_{\mathrm{P}} = \omega_{\mathrm{eg}}$), but use a chirped Gaussian for continuum probing to get a stronger signal

for frequencies far from resonance. By evaluating the different contributions to the signal, shown in figure 3.4, it is evident that the negative delay contribution comes from the perturbed polarization term. Due to regions with negative differential transmission however, the spectrally integrated signal is zero for large negative delays. It should be mentioned that the perturbed polarization depends strongly on the dephasing time. This is treated further in section 3.3.

Another feature of the spectrally resolved signal of figure 3.3 is the areas in delay-frequency space with negative differential transmission. Figure 3.4 shows that the perturbed polarization term is responsible for this feature for large negative delay times. Close to zero delay, both perturbed polarization and polarization coupling contribute to this feature. At these frequencies, the system will therefore exhibit induced absorption rather than induced transmission of the probe for certain delay times.

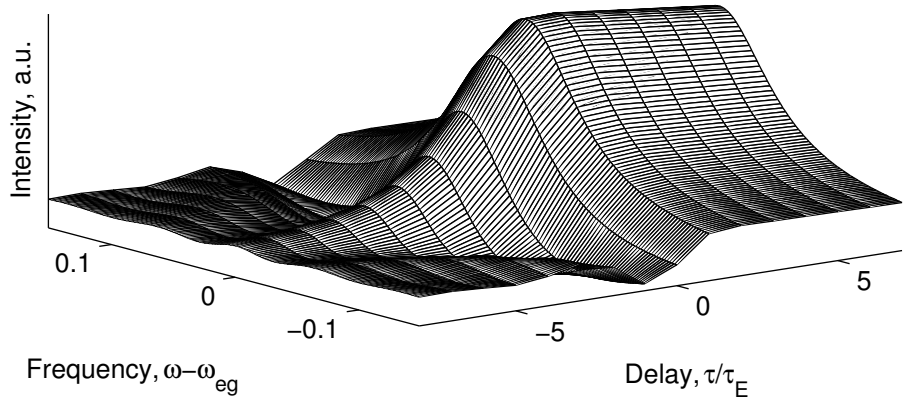


Figure 3.3.: Spectrally resolved on-resonance pump-continuum probe signal.

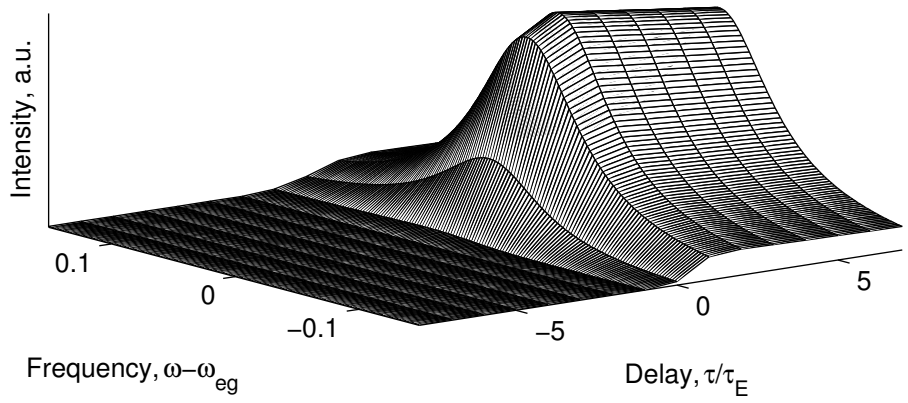


(a) Population term.

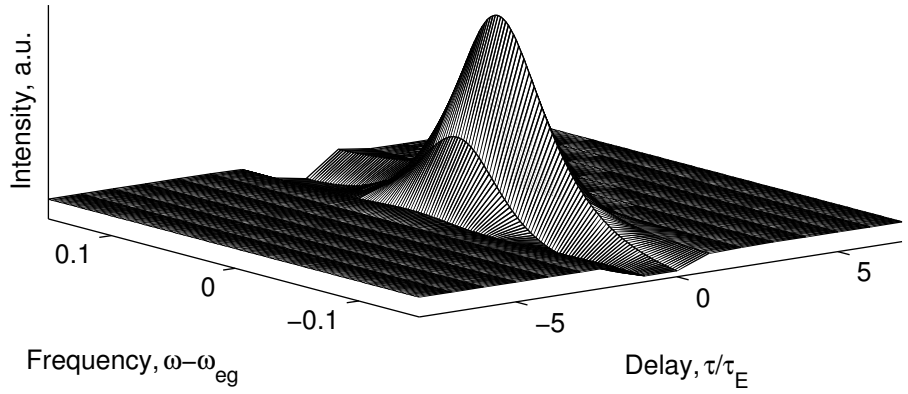


(b) Polarization coupling term.

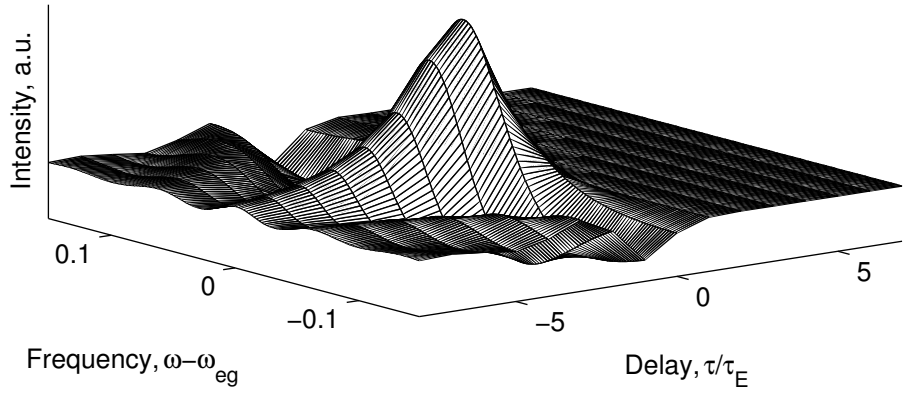


(c) Perturbed polarization term.

Figure 3.4.: Contributions to the spectrally resolved on-resonance pump-continuum probe signal.

We next evaluate the off-resonance response of the two-level system. A pump-continuum probe simulation is chosen, as the system will have a great response for frequencies far from the pump central frequency, $\omega_{\mathrm{P}}$. As we pump off-resonance, the pump-probe signal will naturally be weaker compared to on-resonance pumping. What is more interesting is the shape of the normalized integrated signal, as shown in figure 3.5. The figure gives the normalized pump-continuum probe signal at different offset frequencies $\omega_{\mathrm{P}} - \omega_{\mathrm{eg}}$, with $T_2 = 20\tau_E$. The initial peak in the signal is clearly increasing with the offset.

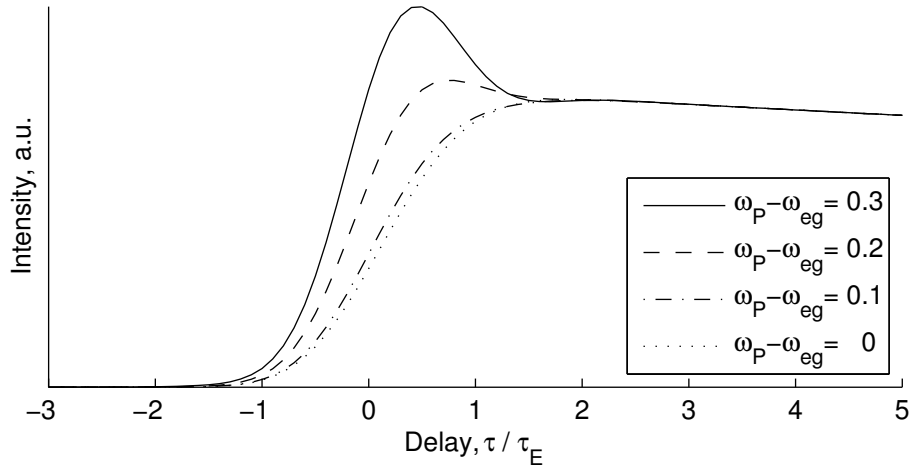


Figure 3.5.: Normalized pump-continuum probe signal at different offset frequencies.

The initial peak has in the on-resonance case been the result of the polarization coupling and perturbed polarization terms. Taking a closer look at the signal contributions for $\omega_{\mathrm{P}} - \omega_{\mathrm{eg}} = 0.3$ shown in figure 3.6 however, the population term also shows a somewhat delayed initial peak. This indicates that the pump excites an additional short-lived population when pumping off-resonance.

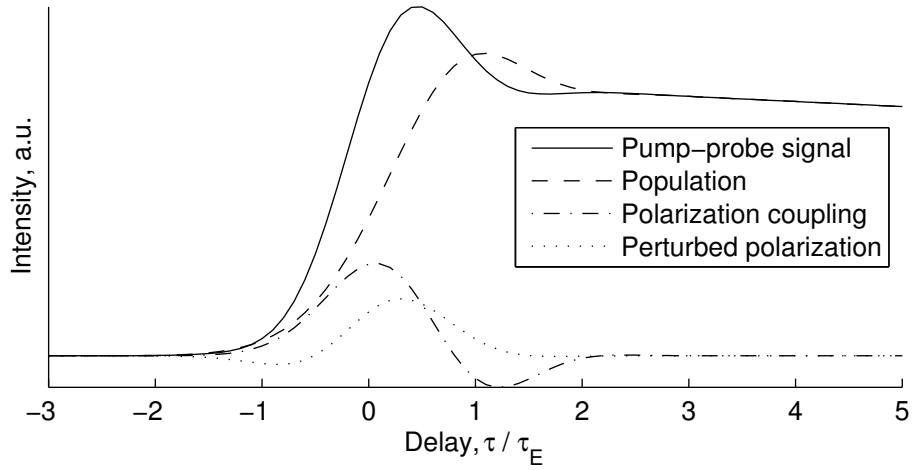


Figure 3.6.: Contributions to the pump-continuum probe signal at offset $\omega_{\mathrm{P}} - \omega_{\mathrm{eg}} = 0.3$.

An interesting feature of figure 3.6 is that the polarization coupling term is negative for short positive delay times, while the perturbed polarization term is negative for short negative delay times. These features are however not easily recognized in the total integrated signal.

The spectrally resolved signal in figure 3.7 shows that off-resonance pumping will still give a signal at the resonance frequency of the signal for long delay times. For shorter delay times on the same time scale as the pump pulse however, the signal is shifted towards the frequency of the pump, with a tail extending towards the pump frequency. The signal shows the same features as the on-resonance signal, but an asymmetry has been introduced with the offset of the field.

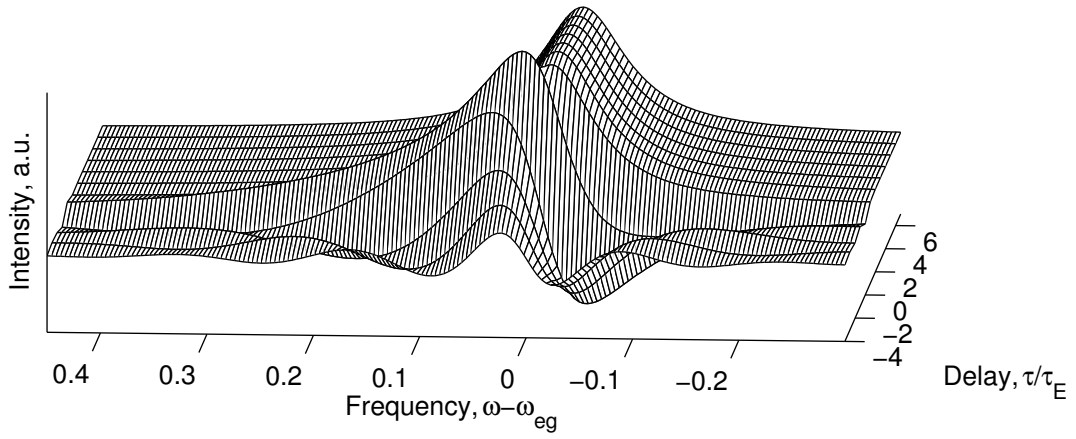


Figure 3.7.: Spectrally resolved pump-continuum probe signal at offset $\omega_{\mathrm{P}} - \omega_{\mathrm{eg}} = 0.3$.

Figure 3.8, giving the contributions to the spectrally resolved signal, shows that the population term, as well as the short lived initial population, is still centered at the resonance frequency of the system. The asymmetry as compared to the on-resonance signal is thus introduced with the polarization coupling and perturbed polarization terms. The rather small negative contributions to the integrated signal are easily recognized as major contributors to the spectrally resolved signal. At frequencies right below resonance, when pumping with a positive offset, there is considerable induced absorption for negative time delays. This feature is greatly enhanced in comparison to the on-resonance signal.

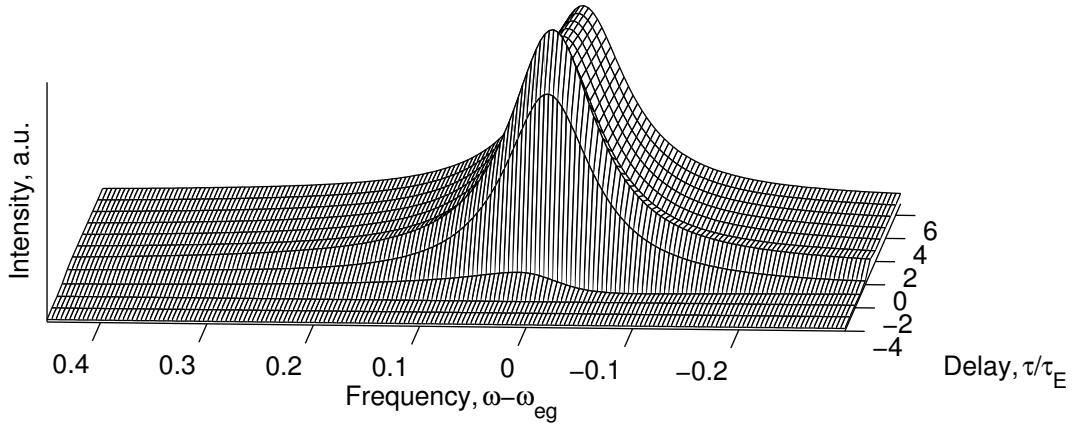


(a) Population term.

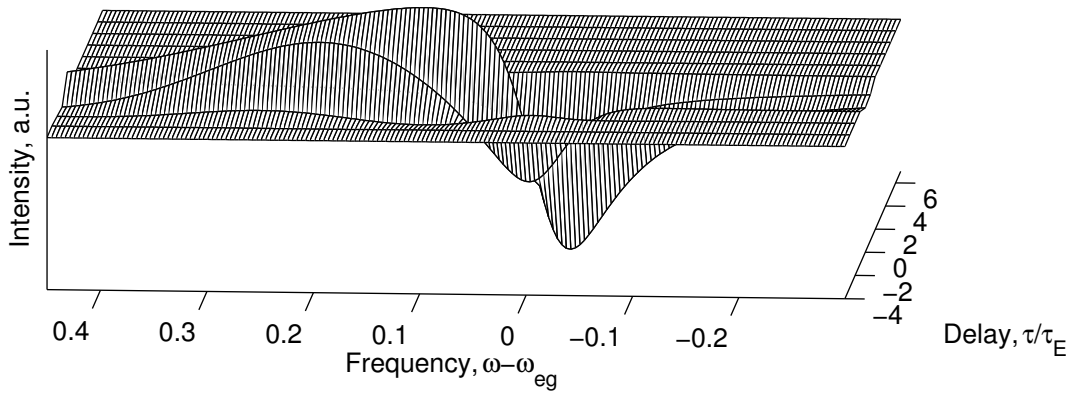


(b) Polarization coupling term.

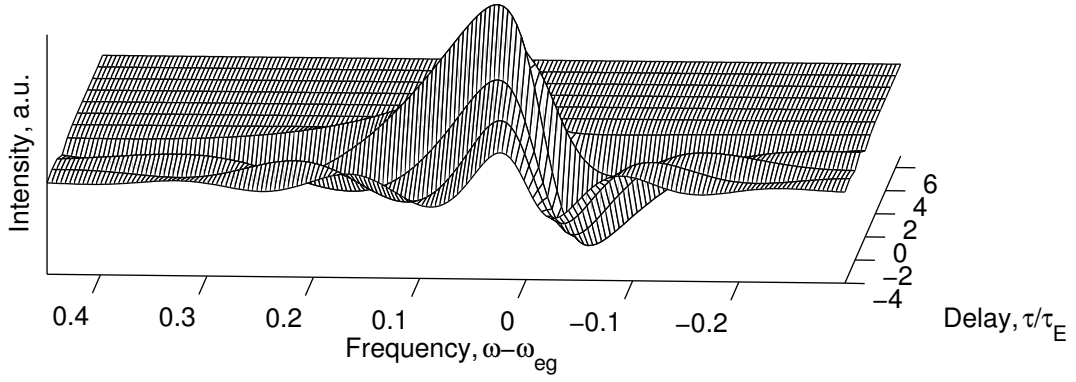


(c) Perturbed polarization term.

Figure 3.8.: Contributions to the spectrally resolved pump-continuum probe signal at offset $\omega_{\mathrm{P}} - \omega_{\mathrm{eg}} = 0.3$.

## 3.3. Extracting Information from the Coherent Signal

The coherent contribution to the pump-probe signal is often referred to as the "coherent artifact", meaning it is just an unwanted spike in the pump-probe signal. It might however be possible to extract some information on the dephasing of the system from the coherent signal. This was proposed by Balk and Fleming [20], and has been further investigated by Chachisvilis et al. [19].

In a system with instantaneous dephasing ($T_2 = 0$) and slow population decay ($T_1 \to \infty$), we have from section 2.3.5 that the coherent signal in a degenerate experiment always gives the electric field autocorrelation squared. The signal is thus symmetrical around zero delay, and only pulse parameters determine the shape of the pulse. With finite dephasing however, the simplifications in section 2.3.5 can not be carried out, and the symmetry breaks down. As shown in figure 3.2, the contribution from Perturbed polarization maintains its symmetry around zero delay, while both the population contribution and the polarization coupling are shifted towards longer delays.

To investigate further, we simulate the pump-probe signal for different dephasing times. The results, consistent with the article by Chachisvilis et al. [19] are illustrated in figure 3.9 for the total pump-probe signal, and figure 3.10 where only the coherent signal is shown. Both figures show scaled signals from degenerate Gaussian pulses of duration $\tau_E$. By increasing the dephasing time, the coherent signal as well as the total signal shifts towards longer delay times. The initial peak in the total signal signal is also greatly reduced for long dephasing times.

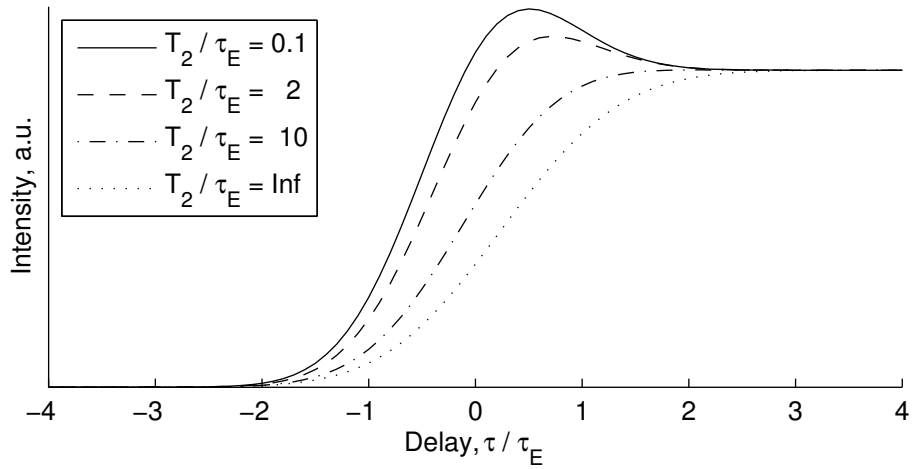


Figure 3.9.: Pump-probe signal for different dephasing times.

As shown in figure 3.3, the spectrally resolved signal can have a considerable signal for negative delays close to the resonance frequency of the system. This signal is greatly affected by the dephasing time which can be seen when evaluating the spectral component of the signal corresponding to system resonance. As shown in figure 3.11a and 3.11b, increasing the dephasing time $T_2$ results in small shifts towards longer delay times $\tau$ to the population and polarization coupling contributions. The greatest change to the

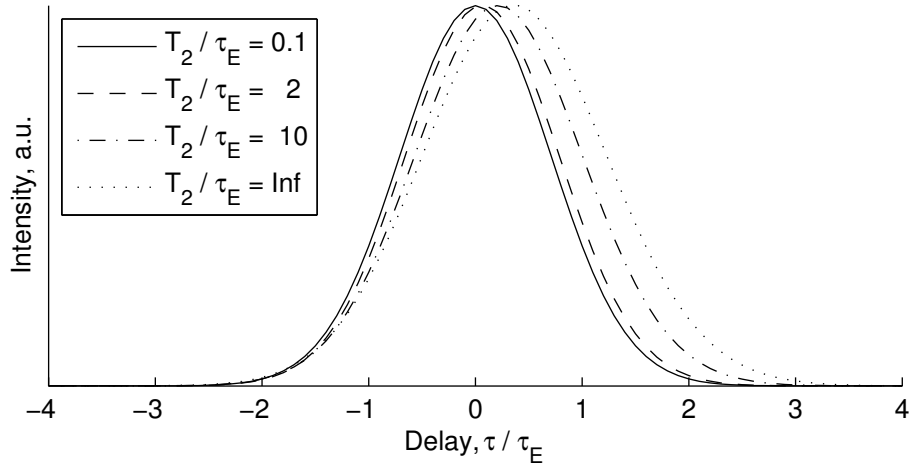


Figure 3.10.: The coherent contribution signal for different dephasing times.

signal however, is the contribution from the perturbed polarization shown in figure 3.11c. Increasing the dephasing time gives a large signal for negative delay times, making it the primary contribution to the spectral component corresponding to system resonance in the pump-probe signal for these delays. As long as the dephasing time is longer than the pulse duration, the shape of this spectral component is determined by the dephasing time. As evident from the figures given so far is this only seen in the spectrally resolved signal, as the perturbed polarisation contribution will cancel at long negative delays when integrating over all frequencies.

Using the dephasing dependence of the signal presented here to extract quantitative information on the dephasing time is however not straightforward. Filtering out only the desired part of the signal is not an easy task, and other processes are likely to influence the signal. Further examples of how the dephasing time may be extracted from the coherent signal are given by Chachisvilis et al. [19], but the same article also emphasizes the risk of overinterpreting data from pump-probe experiments. We will therefore not pursue this further, but refer the interested reader to the original article.

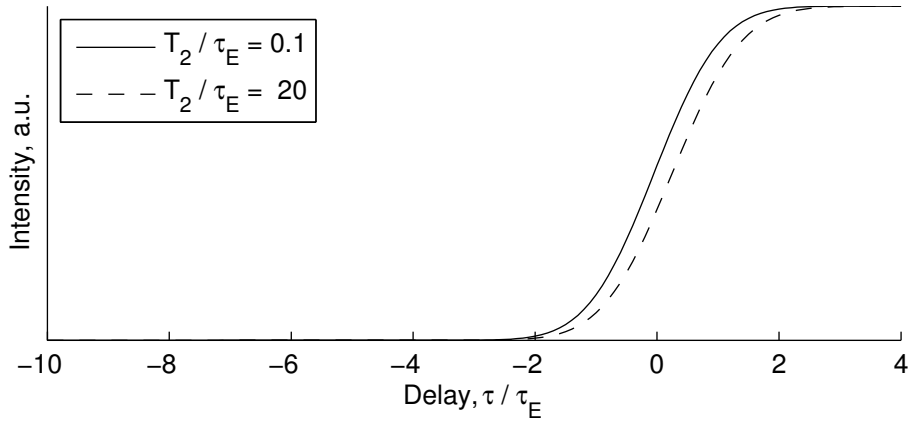


(a) Population term.

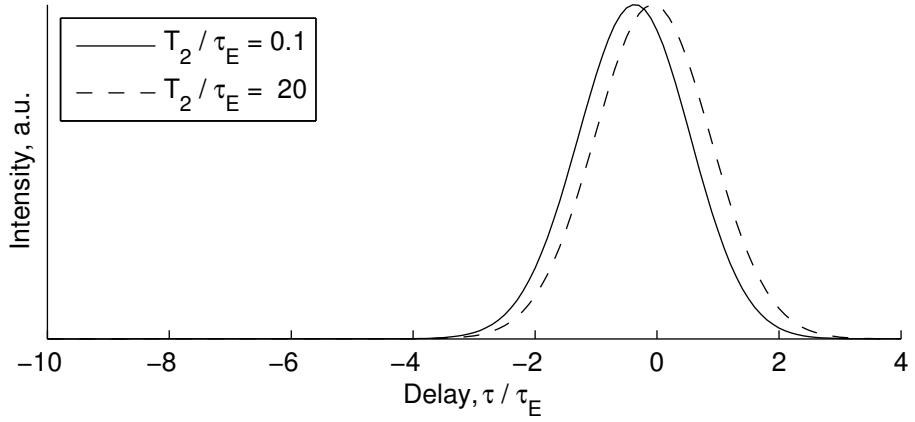


(b) Polarization coupling term.

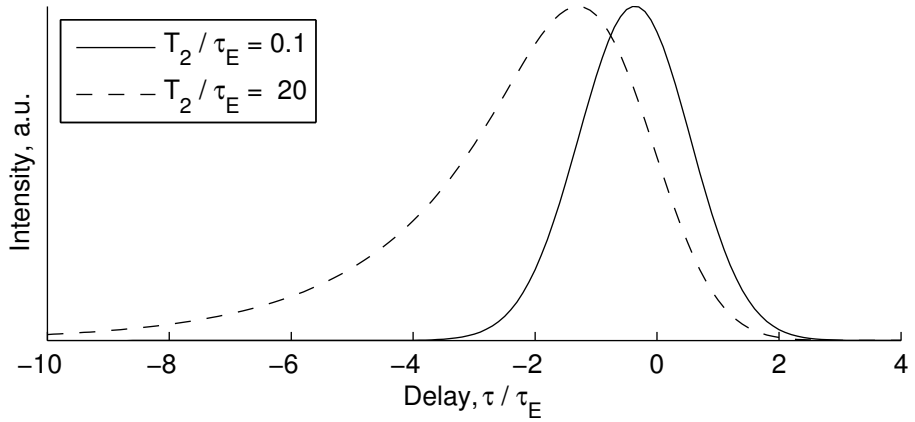


(c) Perturbed polarization term.

Figure 3.11.: Contributions to the spectral component of the pump-probe signal corresponding to the resonance frequency of the system.

## 3.4. Density Matrix Approach - Three-Level System

Degenerate pump-probe experiments of a three-level system with spectrally narrow fields will be no different from the two-level case when relaxation from $|2\rangle$ to $|1\rangle$ is not allowed. The pump will excite either $|1\rangle$ or $|2\rangle$ (or neither), and the test pulse will probe the decay from the excited state to the ground state $|0\rangle$.

A continuum probe however, gives a different result. The simulated signal of pumping of $|2\rangle$ and probing with a continuum pulse is shown in figure 3.12. Only the population term is included, as in the derivation of the expressions in section 2.3.6. It might seem strange that there is a contribution from $|1\rangle$ at all in the figure, as only $|2\rangle$ is pumped. The signal from $|1\rangle$ is however due to the depletion of the ground state, rather than population of $|1\rangle$, which reduces the likeliness of the $|0\rangle \rightarrow |1\rangle$ transition. The high frequency signal is due to both population of $|2\rangle$ and depletion of $|0\rangle$, and is therefore twice the size of the low frequency signal. Pumping of the low state will give identical results, but with $|1\rangle$ contributing twice that of $|2\rangle$.

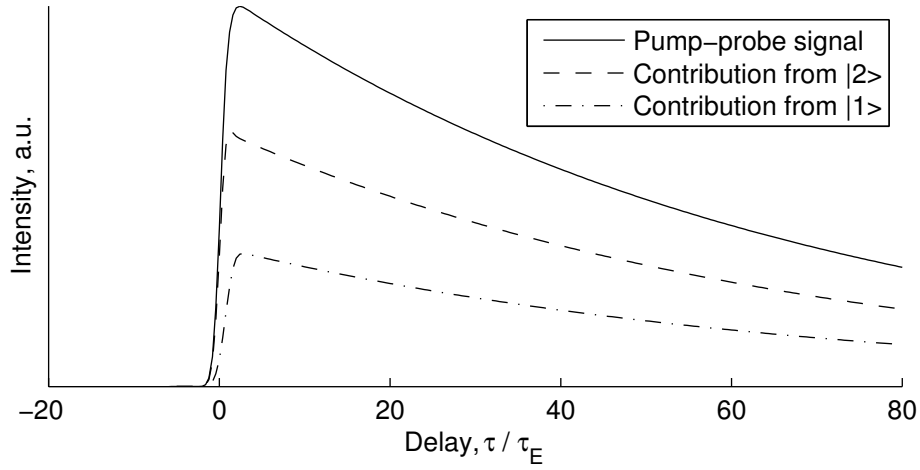


Figure 3.12.: Pump-continuum probe signal when pumping the high level of a three-level system.

The fact that the relaxation of $|2\rangle$ to $|0\rangle$ is the only evolution of the system means the shape of the signal contribution from $|1\rangle$ is determined by the relaxation rate of $|2\rangle$. No information of dynamics of $|1\rangle$ can thus be obtained by pumping $|2\rangle$ when no relaxation from $|2\rangle$ to $|1\rangle$ is allowed.

Another feature of figure 3.12 is the small positive shift of the contribution from $|1\rangle$ compared to that of $|2\rangle$. This is because the continuum probe is modelled as a positively chirped pulse (as in figure 2.3), where high frequencies precede low, so that the high energy transition $|0\rangle \rightarrow |2\rangle$ is probed slightly before the low energy transition $|0\rangle \rightarrow |1\rangle$.

The spectrally resolved signal is shown in figure 3.13. This shows the contributions to the signal at the respective transition frequencies $\omega_{10} = 2$ and $\omega_{20} = 2.5$, and shows the spectral widths of the energy levels, but gives otherwise no additional information to figure 3.12.

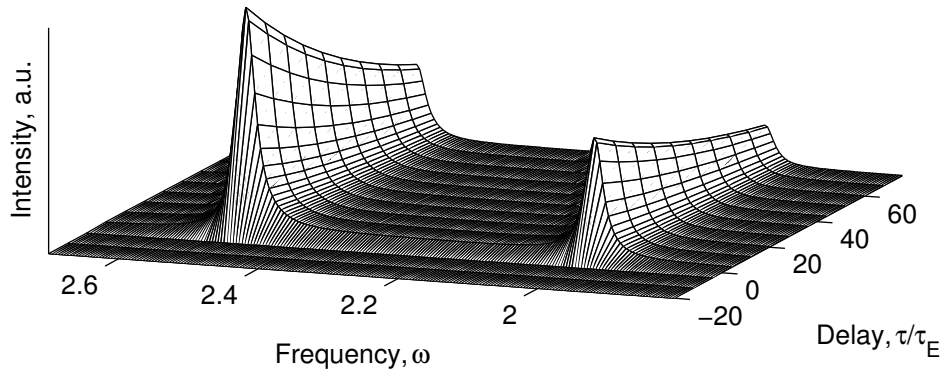


Figure 3.13.: Spectrally resolved pump-continuum probe signal when pumping the high level of a three-level system.

By including relaxation from $|2\rangle$ to $|1\rangle$ as derived in section 2.3.7, a signal rise for long delay times is possible in the spectrally resolved signal. The conditions that need to be fulfilled in obtaining this are a fast $|2\rangle \rightarrow |1\rangle$ transition and a slow $|1\rangle \rightarrow |0\rangle$ transition with $|2\rangle$ decaying mainly to $|1\rangle$ instead of $|0\rangle$ ($\eta_{21} \approx 1$). The integrated signal from the simulation of such a system is shown in figure 3.14 and the spectrally resolved signal in figure 3.15. The total pump-probe signal is still decaying for all positive delays, but the contribution from $|1\rangle$ at $\omega_{10} = 2$ shows an increase after the initial onset before decaying for longer delay times. The contribution from $|2\rangle$ displays a fast decay.

The total pump-probe signal in figure 3.14 can be seen to decay in two steps as it is the sum of the rapidly decaying population in $|2\rangle$ and the slowly decaying population in $|1\rangle$. The two step relaxation occurring at two different rates can therefore be easily recognized even in the frequency integrated signal.

The contributions from $|1\rangle$ and $|2\rangle$ shows resemblance with the highest and lowest energy experimental results in figure 2.14 obtained from GaAs. Although GaAs has energy bands, rather than discrete levels, some of the pump-probe response can thus be reproduced with this simple model. This is however impossible in a two-level model, as the pump-probe signal in that case always will show a constant decay after the initial rise for every frequency probed.

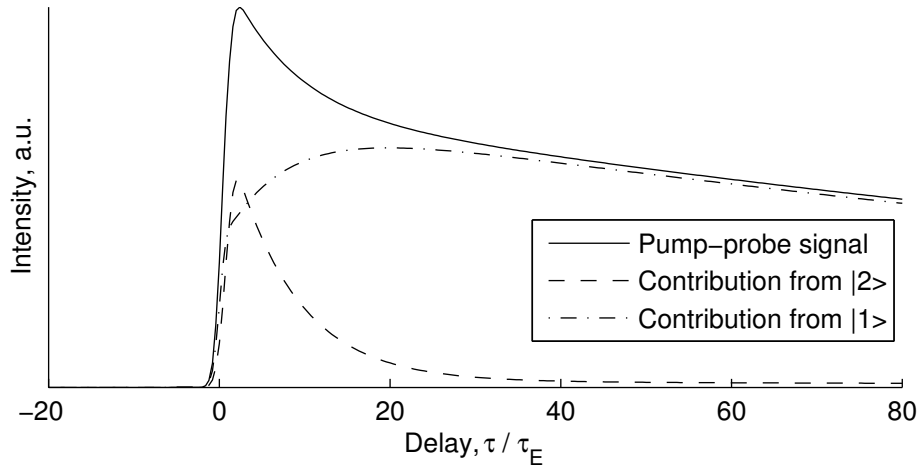


Figure 3.14.: Pump-continuum probe signal when pumping the high level of a three-level system where $|2\rangle \rightarrow |1\rangle$ relaxation is allowed.

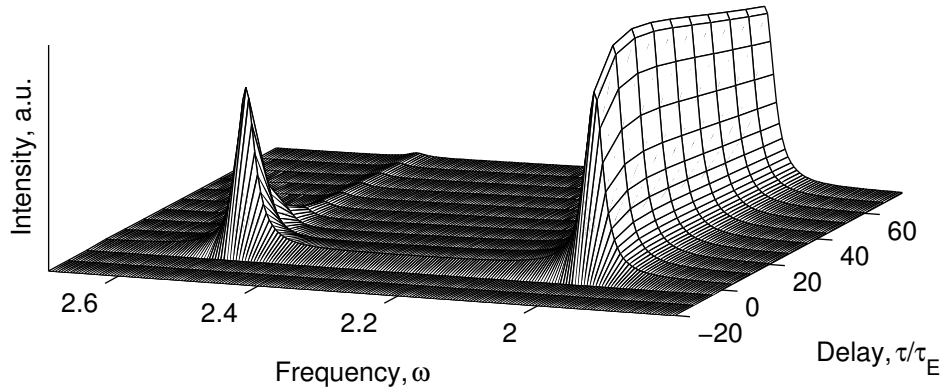


Figure 3.15.: Spectrally resolved pump-continuum probe signal when pumping the high level of a three-level system where $|2\rangle \rightarrow |1\rangle$ relaxation is allowed.

## 3.5. Semiconductor Model

We apply the equations of section 2.5 to simulate the pump-probe signal for a semiconductor.

A Gaussian pump pulse centered at 2 eV with a spectral width of 0.2 eV is chosen. The probe is also a Gaussian pulse centered at 2 eV, but spectrally wider than the pump to detect the pump-probe signal at different energies. To keep it simple, we let $\alpha(\omega)$ be constant for the probed spectrum. We also let the equilibrium hole distribution $N_{\mathrm{h}}^{\mathrm{eq}}(\omega)$ be constant for these energies. The scattering rates $s_{\mathrm{e}}$ and $s_{\mathrm{h}}$ have been set to $0.3/\tau_E$ and $0.15/\tau_E$ respectively such that the electric pulse is short enough that "material properties" determine the signal. These particular parameters have been chosen in an attempt to reproduce the experimental data from section 2.4.1. The result of the simulation is given in figure 3.16 for different probe energies close to the pump energy.

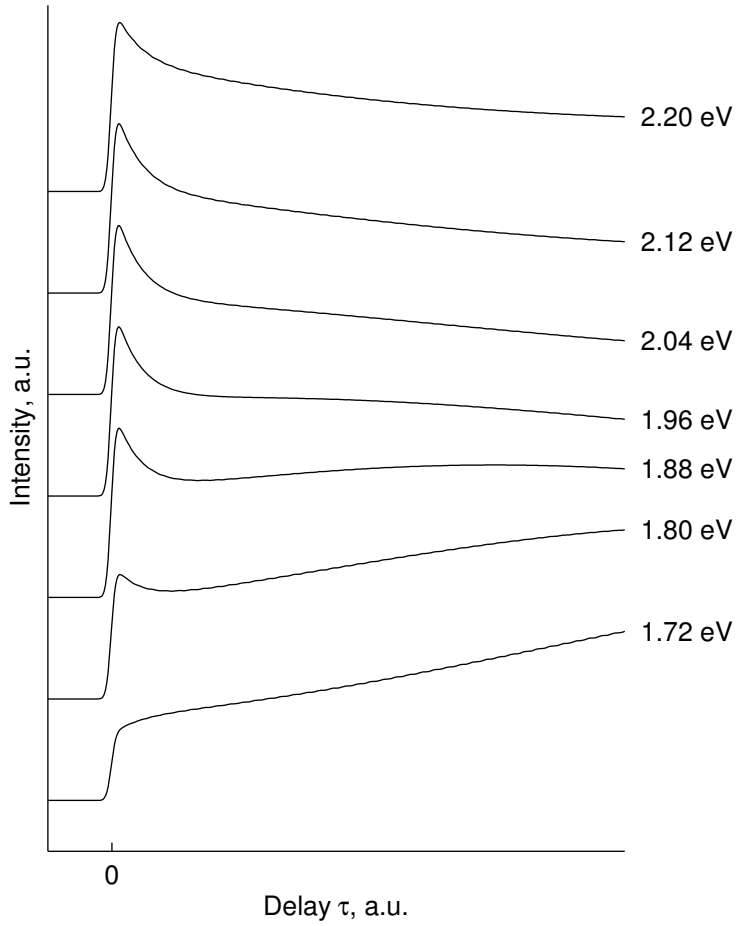


Figure 3.16.: Numerical results for a "semiconductor" pumped at 2 eV, for different probe energies.

Comparison with the experimental data in figure 2.14 shows the same tendency at long delay times of a rising signal for probe energies below the pump energy and decreasing

signal for energies above. For shorter delay times, there is an initial peak for probe energies close to the pump, and an initial rise, but no peak for energies far from the pump. In the articles by Schoenlein et.al. [15, 16] this feature is explained by a hot electron population cooling through electron-electron scattering. In our model however, the peak is the result of fast phonon scattering in a hole band modelled as being flat in energy space.

As the model does not take into account the split-off hole band transition, it fails to reproduce the signal for low energies. We have therefore not included the result for lower energies than 1.72 eV. Already at this energy, there is a mismatch between our result and the experiment. At high energies, the model also fails. While the experimental signal decays to zero, the still large hole population in the model maintains a considerable signal for long delay times.

From the experimental data it is clear that the signal decays at energies above pump energy and rise below pump energy for $\sim$ps delay times. In our model, the signal shows a decay even right below the pump energy. With the assumption of a slowly cooling electron population, the modelled signal will decay even at the pump energy, which seems to be inconsistent with the experimental data. A solution to this may be to include scattering to/from satellite valleys in the model: If we assume that electrons are scattered rapidly by phonons to the X and L valleys by the pump, the satellite valley may function as a reservoir of electrons. These electrons can however not cool significantly, as they are already close to the satellite valley edge as shown in figure 2.13. As the electrons in the $\Gamma$ valley cools however, the satellite valley electrons will return to the $\Gamma$ valley to maintain the balance of electrons between the valleys. This gives a slower decrease of the signal at energies close to the satellite valley edges, in the vicinity of the pump pulse energy.

For energies far from the pump, the model gives a wrong shape for the signal at long delays. The cooling scheme we have chosen gives a late onset of the slow rise for low probe energies and then an escalating growth of the signal for long delays. In the experiment however, the increase in the signal appears to be greatest for short delay times, before flattening out at long delays. This is a weakness in the model resulting from the chosen approach to electron cooling, modelled as a shift in the population energy.

In spite of the weaknesses pointed out, the simple model succeeds in reproducing the main features of the pump-probe signal from GaAs. Bailey et al. [18] have shown how a more sophisticated model gives a result closer to the experiment, but this requires a much more complex evaluation of the system.

## 3.6. Future Work

The work presented on three-level systems in this study is rather limited. A natural continuation of this project would thus be a more general approach to the three-level system, where all terms from the perturbation expansion are included. Coherent signals will then be included in the simulation of the three-level system. Including all terms will also allow for simulation of signals resulting from broad spectrum pumping, and different transition energies than the ones chosen in this study. If this is successfully included in the model, the results should be compared to real systems resembling a three-level

system, hopefully leading to better understanding of relaxation mechanisms in optically excited materials.

There are already great models for explaining pump-probe signals from semiconductors, utilizing Monte Carlo methods [18, 21]. It would however be interesting to investigate how well these models reproduce pump-probe results from more exotic materials, like semiconductor nanowires [22]. These geometries have different properties than and are not as well understood as their bulk counterparts, and are predicted to be important in future semiconductor applications.

# 4. Conclusion

A key point in ultrafast pump-probe spectroscopy is that the pulse used has to be "ultrafast enough". This is quite intuitive, but also explained through the equations governing ultrafast processes given in the theory section of this study, as well as through numerical simulations. With too long pulses, meaning the system response time is as short or shorter than the pulse duration, coherent signals which mainly reflect pulse properties will determine the signal. We have explained the origin of this coherent artifacts in the pump-probe signal, and shown how it can be reduced by reducing the coherence of the pump and probe fields through adding linear chirp to both pump and probe pulses.

Because of the limitations of a classical approach, we have utilized a density matrix approach based on a quantum mechanical treatment of a discrete energy level system. The introduction of a finite dephasing time gives a shift in the population and polarization coupling terms towards longer delay times $\tau$. The perturbed polarization is however not shifted with the introduction of dephasing.

We have shown to a certain degree how the coherent term varies with different dephasing times $T_2$. It is however not straightforward to extract any quantitative information about $T_2$ this way, as other effects may also contribute to the signal in an actual pump-probe experiment. We have also shown how the density matrix approach reduces to the classical result in the case of instantaneous dephasing.

The pump-probe signal, when integrated over all frequencies/energies shows no signal for considerable negative delay times. This is however not the case when evaluating the spectrally resolved signal. We show that close to the resonance frequency of the system, the perturbed polarization contribution will give a large signal at negative delays.

The spectrally resolved signal shows large negative contributions to the transmitted signal at certain frequencies. These contributions originates from the polarization coupling and perturbed polarization terms, especially for values of $\tau$ close to zero. The coherent effects thus produce an induced absorption at these frequencies at short delays rather than the induced transmission one would expect. This effect increases for certain probe frequencies as the system is pumped off-resonance. Pumping off-resonance also excites an additional short-lived population term, as well as introducing an asymmetry to the coherent contributions in the spectrally resolved signal as compared to the on-resonance signal. The signal shows a tail extending towards the pump frequency for short delay times.

We have presented a three-level model for pump-probe, greatly simplified by excluding coherent effects and limiting to spectrally narrow pump pulses. When pumping the high level in the three-level system and probing with a continuum pulse, there will be a signal at both frequencies, with the high frequency signal twice that of the low frequency signal. This is due to the fact that both depletion of the ground state as well as population of the higher energy states contribute to the signal

By including relaxation between level $|2\rangle$ and $|1\rangle$, we have shown how a sustained increase in the pump-probe spectrum at a certain frequency is possible. The result resembles experimental results from GaAs. A two-step decay process is also clearly evident in the integrated pump-probe signal

A simple model for the populations of the energy bands of a semiconductor is introduced, and we show how this is related to the well established density matrix approach. The model succeeds in reproducing the main features in experimental data from pump-probe of GaAs, but a good fit to the experimental data requires a more sophisticated model.

# Bibliography


[1] L. L. Endelman, "A brief history of high speed photography 1851-1930." Part of the High Speed Photography Retrospective during the SPIE's 32nd Annual International Technical Symposium, 1988.

[2] A. M. Weiner, "Ultrafast Time-Resolved Spectroscopy," in *Ultrafast Optics*, pp. 422–506, John Wiley & Sons, Inc., 2008.

[3] W. Z. Lin, L. G. Fujimoto, E. P. Ippen, and R. A. Logan, "Femtosecond carrier dynamics in GaAs," *Applied Physics Letters*, vol. 50, no. 3, pp. 124–126, 1987.

[4] R. L. Fork, C. V. Shank, C. Hirlimann, R. Yen, and W. J. Tomlinson, "Femtosecond white-light continuum pulses," *Opt. Lett.*, vol. 8, pp. 1–3, Jan 1983.

[5] B. E. A. Saleh and M. C. Teich, *Fundamentals of photonics*. Wiley series in pure and applied optics, Wiley-Interscience, 2nd ed., 2007.

[6] Y. Shen, *The principles of nonlinear optics*. Wiley Series in Pure and Applied Optics, J. Wiley, 1984.

[7] S. Mukamel, *Principles of Nonlinear Optical Spectroscopy*. Oxford series on optical sciences, Oxford University Press, 1999.

[8] E. P. Ippen and C. V. Shank, "Techniques for picosecond measurement," in *Ultrashort light pulses : picosecond techniques and applications* (S. L. Shapiro, ed.), Springer-Verlag, New York, 1977.

[9] Z. Vardeny and J. Tauc, "Picosecond coherence coupling in the pump and probe technique," *Optics Communications*, vol. 39, no. 6, pp. 396 – 400, 1981.

[10] M. Joffre, "Coherent effects in femtosecond spectroscopy: A simple picture using the bloch equation," in *Femtosecond Laser Pulses* (C. Rullière, ed.), Advanced Texts in Physics, pp. 283–308, Springer New York, 2005.

[11] B. Bransden and C. Joachain, *Quantum mechanics*. Prentice Hall, 2000.

[12] B. Streetman and S. Banerjee, *Solid State Electronic Devices*. Prentice Hall Series in Solid State Physical Electronics, Pearson Prentice-Hall, 2009.

[13] S. Richard, F. Aniel, and G. Fishman, "Energy-band structure of Ge, Si, and GaAs: A thirty-band $\mathbf{k} \cdot \mathbf{p}$ method," *Phys. Rev. B*, vol. 70, p. 235204, Dec 2004.

[14] R. Schoenlein, W. Lin, S. Brorson, E. Ippen, and J. Fujimoto, "Femtosecond hot carrier energy redistribution in GaAs and AlGaAs," *Solid-State Electronics*, vol. 31, no. 3-4, pp. 443 – 446, 1988.

[15] R. W. Schoenlein, W. Z. Lin, E. P. Ippen, and J. G. Fujimoto, "Femtosecond hot-carrier energy relaxation in GaAs," *Applied Physics Letters*, vol. 51, no. 18, pp. 1442–1444, 1987.

[16] W. Z. Lin, R. W. Schoenlein, J. G. Fujimoto, and E. P. Ippen, "Femtosecond absorption saturation studies of hot carriers in GaAs and AlGaAs," *Quantum Electronics, IEEE Journal of*, vol. 24, pp. 267 –275, feb 1988.

[17] A. Othonos, "Probing ultrafast carrier and phonon dynamics in semiconductors," *Journal of Applied Physics*, vol. 83, no. 4, pp. 1789–1830, 1998.

[18] D. W. Bailey, C. J. Stanton, and K. Hess, "Numerical studies of femtosecond carrier dynamics in GaAs," *Phys. Rev. B*, vol. 42, pp. 3423–3434, Aug 1990.

[19] M. Chachisvilis, H. Fidder, and V. Sundström, "Electronic coherence in pseudo two-colour pump-probe spectroscopy," *Chemical Physics Letters*, vol. 234, no. 1–3, pp. 141–150, 1995.

[20] M. W. Balk and G. R. Fleming, "Dependence of the coherence spike on the material dephasing time in pump–probe experiments," *The Journal of Chemical Physics*, vol. 83, no. 9, pp. 4300–4307, 1985.

[21] D. W. Bailey and C. J. Stanton, "Calculations of femtosecond differential optical transmission in germanium," *Journal of Applied Physics*, vol. 77, no. 5, pp. 2107–2115, 1995.

[22] R. P. Prasankumar, P. C. Upadhya, and A. J. Taylor, "Ultrafast carrier dynamics in semiconductor nanowires," *physica status solidi (b)*, vol. 246, no. 9, pp. 1973–1995, 2009.

# A. Appendix

## A.1. Green's Functions and ODEs

We look at a general, inhomogeneous, first order ODE and define the operator $L$ as

$$L[y] \equiv y' + p(x)y = f(x), \qquad x > a. \tag{A.1}$$

We also introduce the boundary condition

$$B[y] \equiv y(a) = 0, \tag{A.2}$$

and define the Green's function $G(x|\xi)$ as

$$L[G(x|\xi)] = G' + p(x)G = \delta(x - \xi), \tag{A.3}$$
$$B[G(x|\xi)] = G(a|\xi) = 0. \tag{A.4}$$

This leads to the following identities

$$\begin{aligned} L\left[\int_a^\infty G(x|\xi)f(\xi)d\xi\right] &= \int_a^\infty L\left[G(x|\xi)\right] f(\xi)d\xi \\ &= \int_a^\infty \delta(x-\xi)f(\xi)d\xi \\ &= f(x), \end{aligned} \tag{A.5}$$

and

$$\begin{aligned} B\left[\int_a^\infty G(x|\xi)f(\xi)d\xi\right] &= \int_a^\infty B\left[G(x|\xi)\right] f(\xi)d\xi \\ &= \int_a^\infty (0)f(\xi)d\xi \\ &= 0, \end{aligned} \tag{A.6}$$

so that

$$y(x) = \int_a^\infty G(x|\xi)f(\xi)d\xi. \tag{A.7}$$

We evaluate $L[G]$:

$$G' + p(x)G = \delta(x - \xi), \tag{A.8}$$

and integrate in the tiny interval $\xi \in [\xi^-, \xi^+]$ to get

$$G(\xi^+|\xi) - G(\xi^-|\xi) + \int_{\xi^-}^{\xi^+} p(x)G(x|\xi)dx = 1. \tag{A.9}$$

As the limits $\xi^-$ and $\xi^+$ approach each other, the integral becomes zero, and we end up with

$$G(\xi^+|\xi) - G(\xi^-|\xi) = 1. \tag{A.10}$$

For all $x \neq \xi$, we have the homogeneous solution

$$G(x|\xi) = \begin{cases} c_1 e^{-\int p(x)dx}, & a < x < \xi, \\ c_2 e^{-\int p(x)dx}, & \xi < x, \end{cases} \tag{A.11}$$

and since $G(a|\xi) = 0$, $c_1$ has to be 0 which gives

$$G(x|\xi) = \begin{cases} 0, & a < x < \xi, \\ c_2 e^{-\int p(x)dx}, & \xi < x. \end{cases} \tag{A.12}$$

Furthermore, the equation above gives that $G(\xi^+|\xi) = 1$, which determines the integration limits, and the constant $c_2$ such that

$$G(x|\xi) = \begin{cases} 0, & a < x < \xi, \\ e^{-\int_\xi^x p(t)dt}, & \xi < x. \end{cases} \tag{A.13}$$

or, using the Heaviside step function $\Theta(x)$,

$$G(x|\xi) = \Theta(x - \xi)\, e^{-\int_\xi^x p(t)dt}. \tag{A.14}$$

If $p(x)$ is a constant $p(x) = C$, this yields

$$G(x|\xi) = \Theta(x - \xi)\, e^{-C(x-\xi)} = G(x - \xi). \tag{A.15}$$

As $G(x < a) = 0$, the solution to the ODE is

$$\begin{aligned} y(x) &= \int_a^\infty G(x|\xi) f(\xi) d\xi \\ &= \int_{-\infty}^\infty G(x - \xi) f(\xi) d\xi \\ &= G(x) \otimes f(x). \end{aligned} \tag{A.16}$$

## A.2. Feynman Diagrams

The double sided Feynman diagram is a way of representing the interaction of the electric field with the density matrix. The diagram represents the density matrix as two vertical lines, where the left-hand line is the ket $|n\rangle$ and the right-hand line is the bra $\langle m|$. A photon interacting with the system is represented as a wavy arrow on either the ket or bra side of the diagram, resulting in a transition of the density matrix to the next order in the electric field represented by a horizontal line, as shown in figure A.1. When using complex notation, so that $E(t) = \mathrm{Re}\{\mathcal{E}(t)\}$, an arrow pointing right represents $\mathcal{E}(t)$, while an arrow pointing left represents $\mathcal{E}^*(t)$. The evolution of the matrix element $\rho_{nm}(t)$ between interactions is governed by a convolution with the Green's function $G_{nm}(t)$. These conventions make it easy to write down the equation for the density matrix by looking at the corresponding Feynman diagram.

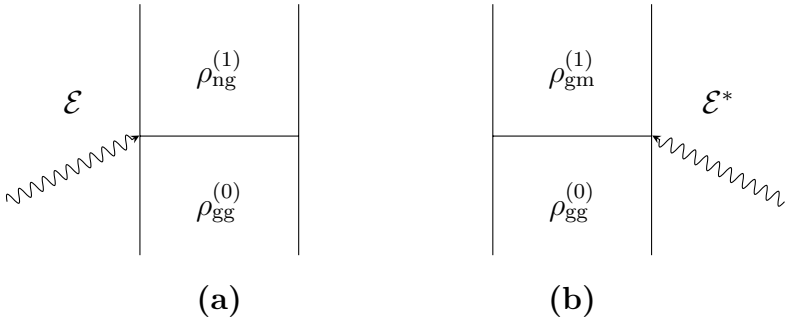


Figure A.1.: Excitation on the left(a) and right(b) side of a Feynman diagram.

By constructing the Feynman diagrams corresponding to the terms in the expressions for the density matrix elements, it is easy to evaluate whether or not a term contributes in the rotating wave approximation. We use the following rule: In figure A.2a, the ket $|\mathrm{g}\rangle$ absorbs a photon, and goes into state $|n\rangle$, which conserves the energy of the system as a whole. In figure A.2b however, the ket $|\mathrm{g}\rangle$ emits a photon as it goes into state $|n\rangle$, giving an energy mismatch of twice the photon energy. Therefore, this term does not contribute in the rotating wave approximation.

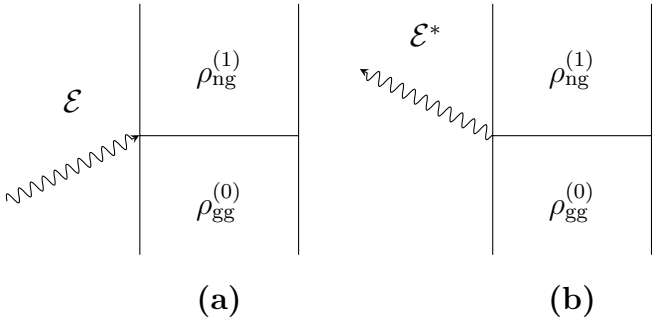


Figure A.2.: Diagram (a) contributes in the RWA, while (b) does not.